PASSIVE RANGE ESTIMATION FOR ANTISHIPPING MISSILES

James H. Taylor, et al

Analytic Sciences Corporation

Prepared for:

Office of Naval Research

1 December 1975

ONR-CR215-214-4F

PASSIVE RANGE ESTIMATION FOR ANTISHIPPING MISSILES

James H. Taylor and Charles F. Price
THE ANALYTIC SCIENCES CORPORATION
Six Jacob Way
Reading, Massachusetts 01867

15 March 1976

Final Report for the Period
1 February 1973 - 31 December 1975

Prepared for

THE OFFICE OF NAVAL RESEARCH
Vehicle Technology Program, Code 211
Arlington, Virginia 22217

When this report is no longer needed, it may be transmitted to other organizations. Do not return it to the originator or the monitoring office.

The findings in this report are not to be construed as an official Department of Defense or Military Department position.

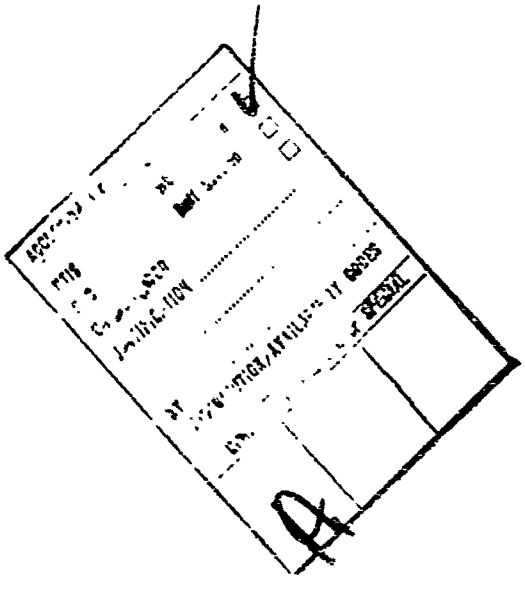

UNCLASSIFIED

SECURITY CLASSIFICATION OF THIS PAGE (When Data Entered)

REPORT DOCUMENTATION PAGE		READ INSTRUCTIONS BEFORE COMPLETING FORM
1. REPORT NUMBER ONR-CR215-214-4F	2. GOVT ACCESSION NO.	3. RECIPIENT'S CATALOG NUMBER
4. TITLE (and Subtitle) PASSIVE RANGE ESTIMATION FOR ANTISHIPPING MISSILES		5. TYPE OF REPORT & PERIOD COVERED Final Technical Report 1 Feb. 1973 - 31 Dec. 1975 6. PERFORMING ORG. REPORT NUMBER TR-385-4
7. AUTHOR(s) James H. Taylor Charles F. Price		8. CONTRACT OR GRANT NUMBER(s) N00014-73-C-0213
9. PERFORMING ORGANIZATION NAME AND ADDRESS The Analytic Sciences Corp. Six Jacob Way Reading, Mass. 01867		10. PROGRAM ELEMENT, PROJECT, TASK AREA & WORK UNIT NUMBERS
11. CONTROLLING OFFICE NAME AND ADDRESS The Office of Naval Research Vehicle Technology Program, Code 211 Arlington, Virginia 22217		12. REPORT DATE 1 December 1975 13. NUMBER OF PAGES 70
14. MONITORING AGENCY NAME & ADDRESS(if different from Controlling Office)		15. SECURITY CLASS. (of this report) UNCLASSIFIED 15a. DECLASSIFICATION DOWNGRADING SCHEDULE

16. DISTRIBUTION STATEMENT (of this Report)

Distribution of this report is unlimited

17. DISTRIBUTION STATEMENT (of the abstract entered in Block 20, if different from Report)

18. SUPPLEMENTARY NOTES

19. KEY WORDS (Continue on reverse side if necessary and identify by block number)

Passive Range Estimation
Nonlinear Filtering
Missile Guidance Systems

20. ABSTRACT (Continue on reverse side if necessary and identify by block number)

This report deals with several techniques for passive ranging, i.e., the estimation of target range from noisy measurements of bearing or line-of-sight angle alone. The type of engagement treated in this investigation involves a maneuvering surface target and a missile without an altimeter. The missile approaches the target along a trajectory that is characterized by a low-altitude cruise phase followed by a(Cont)

DD FORM 1 JAN 73 1473 EDITION OF 1 NOV 65 IS OBSOLETE

UNCLASSIFIED

SECURITY CLASSIFICATION OF THIS PAGE (When Data Entered)

ABSTRACT (Continued)

terminal pitch-up maneuver. Several modified Kalman filter-like algorithms are applied to this nonlinear filtering problem; these include the extended Kalman filter (based on small-signal linearization) and several quasi-linear Kalman filters (based on random-input describing function theory). Performance comparisons are obtained by applying the filters to a number of trajectories.

TABLE OF CONTENTS

LIST OF FIGURES

LIST OF TABLES

1. INTRODUCTION

1.1 BACKGROUND

A tactical missile guidance system may require an accurate estimate of missile-target range. Acceptable accuracy can usually be achieved using direct radar range measurement techniques. However, it is a distinct possibility that radar range information may not be available, either due to electronic jamming by the hostile target, or due to the use of a passive seeker (with infrared or electro-optical sensors, for example).* In either case, the missile guidance system will generally be able to measure target bearing or line-of-sight (LOS) angle. It is thus important to develop passive range estimation techniques, based on the assumption that LOS angle is the only information available regarding the relative position of the target from the missile.

One application where range estimation is of interest is a homing guidance system attempting to intercept a surface target (land or sea). A recent feasibility study undertaken at TASC has demonstrated that a sophisticated, inertially-aided, data processing algorithm (filter) can provide quite accurate estimates of range in an antishipping missile application when the missile performs a terminal pitch-up maneuver (Ref. 1). In that investigation, an

*If it is anticipated that range measurements may be denied by jamming, then a home-on-jam capability can be incorporated in the target tracking system, while passive seekers are specifically designed to provide LOS angle information.

extended Kalman filter was provided with measurements of LOS angle, missile acceleration, missile altitude, and missile attitude. Range estimation was greatly facilitated by the terminal missile pitch-up maneuver performed to achieve an advantageous target approach angle. Furthermore, the success of the extended Kalman filter was due in part to the assumption that initial estimation errors were relatively small -- as might be the case if radar range measurements were available up to the filter initialization time.

In many missile guidance situations, it is important to be able to obtain good range estimates at relatively long ranges were LOS angular excursions are small. If it is necessary to perform a terminal maneuver, for example, it would be important to initiate the maneuver at the correct missile-target separation. It may also be necessary to have an accurate passive ranging capability when initial range estimates are poor. These requirements provide the motivation for the present detailed investigation of passive range estimation algorithms.

The essentials of the problem under consideration are depicted in Fig. 1.1-1. In this study, the equations of motion are expressed in Cartesian coordinates, x and y, representing missile-target separation. This formulation leads to system dynamics that can be approximated with a linear model, and to a measurement equation that contains the nonlinearity

$$\theta = \tan^{-1}(y/x) \qquad (1.1\text{-}1)$$

where θ is the LOS angle. While the use of polar coordinates would lead to a linear measurement equation, the system dynamic equations that result contain a number of highly nonlinear terms. Cartesian coordinates are chosen so that attention

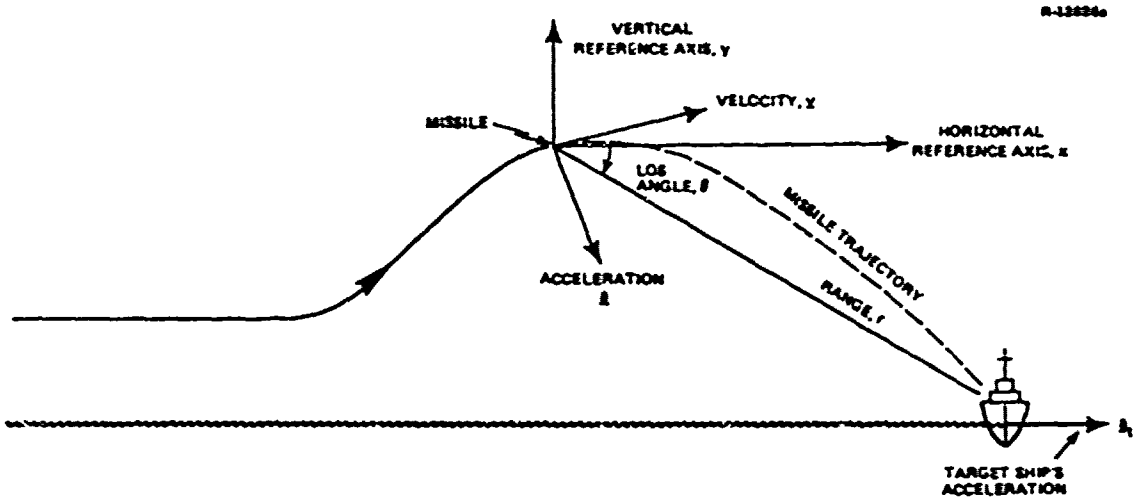

Figure 1.1-1 Missile-Ta · Intercept Geometry

can be restricted to a single dominant nonlinearity--the LOS angle measurement equation indicated in Eq. (1.1-1). An additional secondary nonlinear effect that may appear in the above measurement equation is LOS angle quantization. The impact of LOS angular quantization on the range estimation problem is studied here as well.

It is assumed that the measurement data consists of noisy measurements of θ and noise-free measurements of the missile acceleration. The motion of the target (ship) is modeled as a horizontal acceleration vector, $\underline{a}_t$, with a magnitude that is a correlated gaussian random process with bandwidth and rms value selected appropriately. Mathematical details concerning the system model may be found in Chapter 2.

The above paragraphs outline the motivation for, and provide an overview of, the range estimation problem considere in this investigation. In the next section, an outline of possible filter design techniques that may fulfill the need for accurate estimates of missile-target separation is presented.

1.2 TECHNICAL APPROACH

The optimal estimation problem for linear systems has been solved (Ref. 2). The well-known Kalman filter algorithm results in a set of recursive relations with which each measurement can be processed to yield an updated estimate of the system variables of interest. The estimate provided by the Kalman filter is optimal, in the sense that the variance of the estimation error is minimized. One essential property of this approach is that an exact replica of the linear system model is incorporated in the algorithm; the performance of the filter is impaired if this model inaccurately reflects the real world. The relation between the linear system model and the optimal Kalman filter is portrayed in Fig. 1.2-1

While the technique outlined above has proven to be very successful in applications where the assumption of linearity is realistic, the extension of optimal estimation methodology to the nonlinear case is not necessarily straightforward. A widely-used solution to the nonlinear filtering problem is the extended Kalman Filter (Ref. 2); it is depicted in Fig. 1.2-2 in the same conceptual terms as the Kalman filter shown in Fig. 1.2-1. The implementation of the resulting algorithm calls for replacing all system nonlinearities with linear gains that are equal to the slopes of the nonlinearities; the slopes are computed at the present estimate of the system variables, $\hat{\underline{x}}$. This procedure is called small-signal linearization about the current estimate. It is accurate (i.e., provides a realistic system model for incorporation in the filter algorithm) as long as estimation error is small and changes in the slopes of the nonlinearities are small over the region of interest. Clearly, these conditions may be restrictive, and they

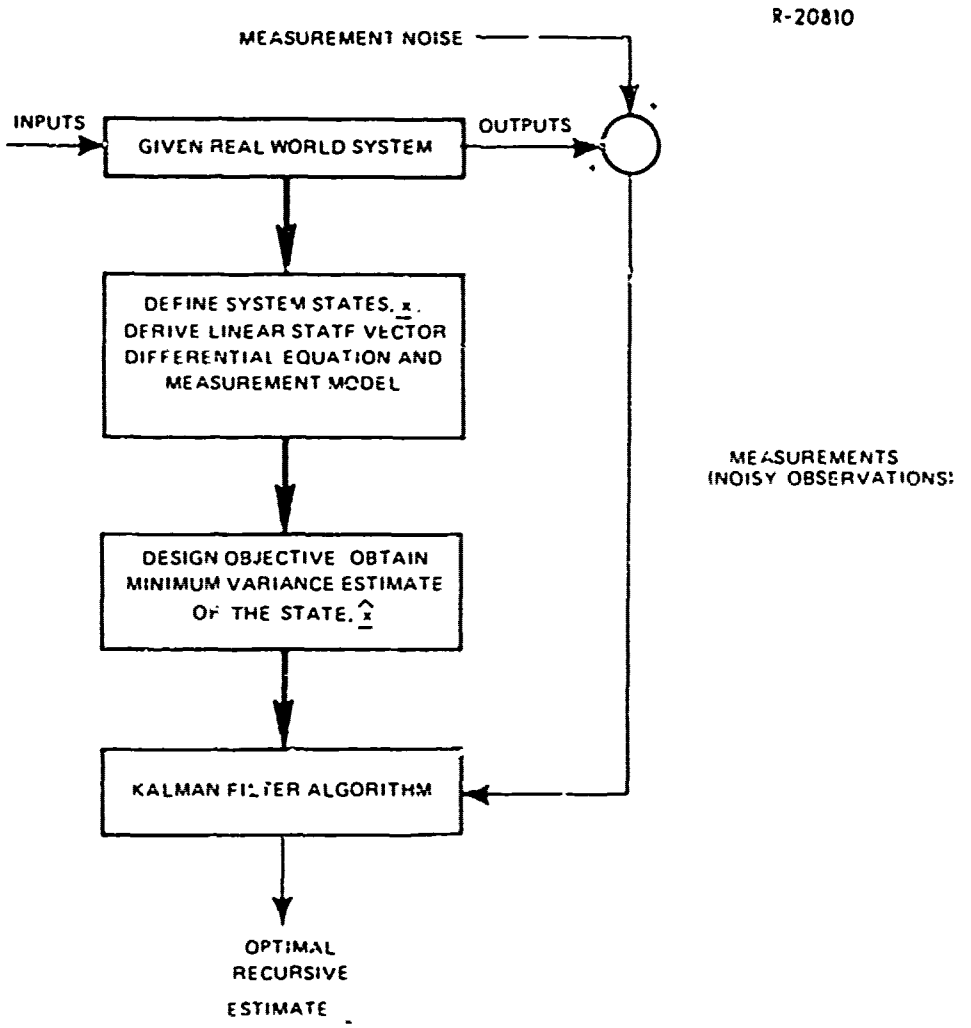

Figure 1.2-1 Kalman Filter Design Principles for Linear Systems

raise questions as to how "small" the estimation error and slope variations must be, and how much the filter performance is degraded when the conditions are violated. Nonetheless, there have been many applications in which the extended Kalman filter has proven to be effective.

If the underlying assumptions of the extended Kalman filter design approach are questionable, as may be the case in applications of the sort considered here, then more sophisticated solutions to the nonlinear filtering

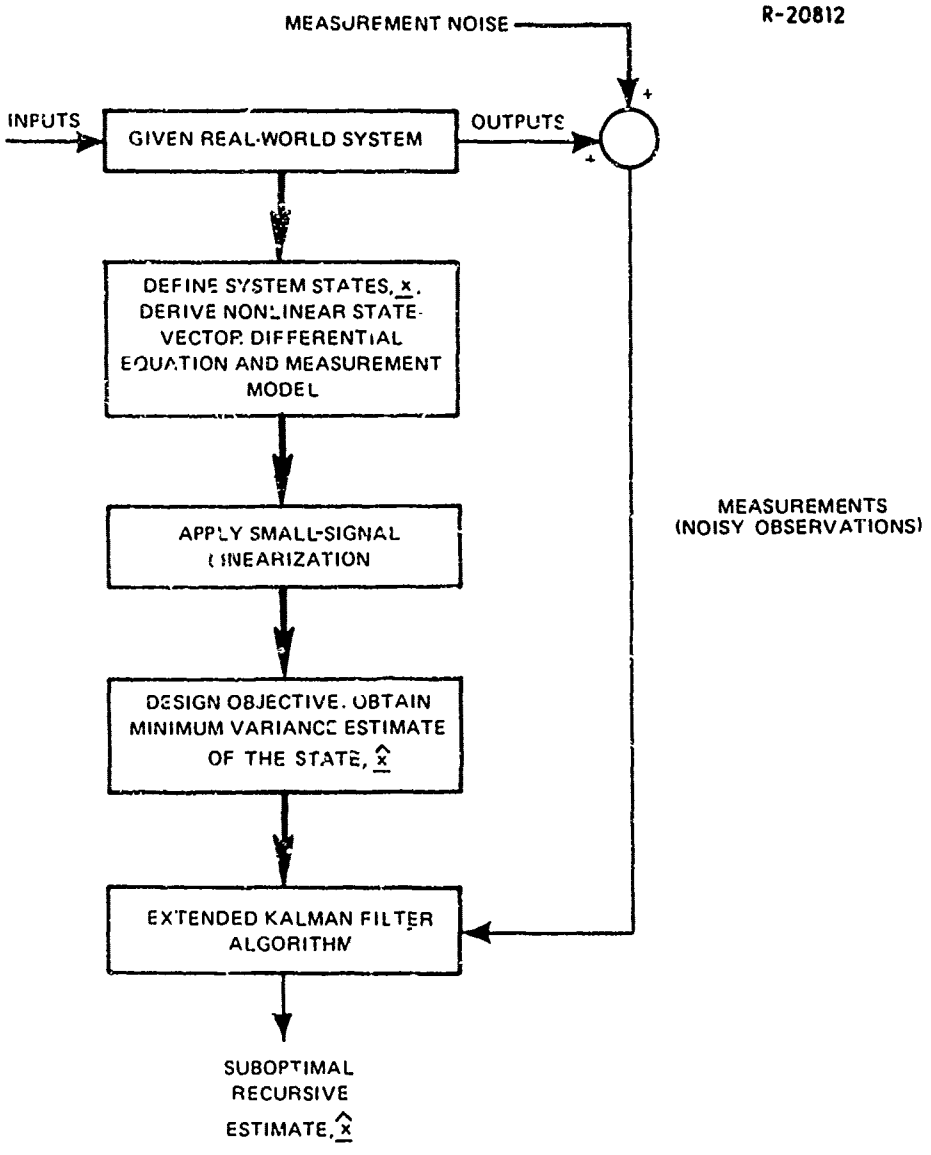

Figure 1.2-2 Extended Kalman Filter Design Principles for Nonlinear Systems

problem could be required. One possible approach is based on describing function theory, and can be called the quasi-linear Kalman filter design. This concept, which involves replacing each system nonlinearity with a random-input describing function (Ref. 3), is illustrated in Fig. 1.2-3; it is an alternative design technique investigated in this study.

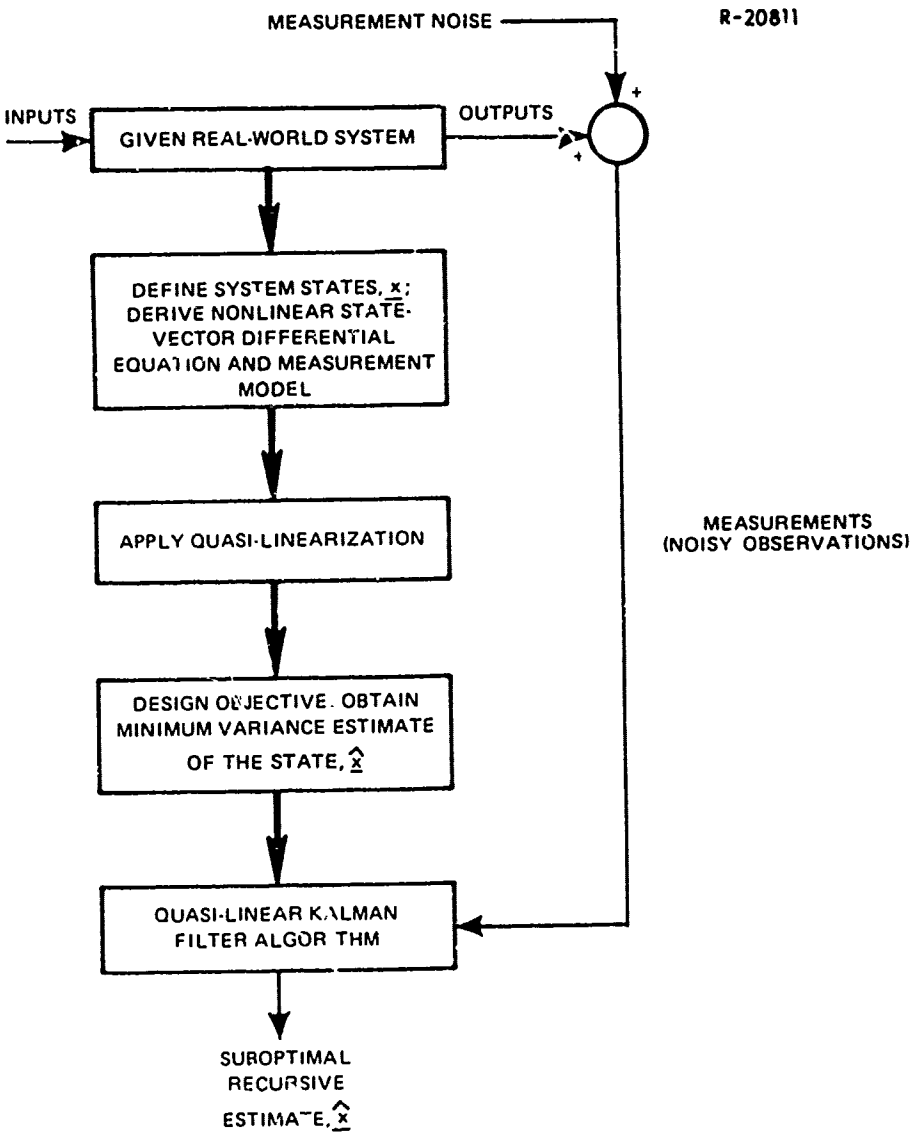

Figure 1.2-3 Quasi-Linear Kalman Filter Design Principles for Nonlinear Systems

The fact that nonlinear filtering is not amenable to a unified, dependable methodology is compensated to some extent by the existence of the Cramér-Rao inequality. In some instances, this inequality defines lower bounds on the filter estimation error variance that can be achieved by the best possible filter, even if such a filter is unknown.

Given a Cramer-Rao lower bound on achievable estimation error variance, it is possible to assess how well existing filters are performing a specific nonlinear filtering task. If a candidate filter provides estimation errors that are comparable to the Cramér-Rao lower bound, then there is little to be gained by using other algorithms.

The goal of this investigation is to determine the performance of the extended Kalman filter and of several forms of the quasi-linear Kalman filter in the range estimation problem outlined in Section 1.1. Direct comparison of the performance of these filter algorithms provides a great deal of insight into their strengths and weaknesses, and the Cramér-Rao inequality is useful in assessing their absolute performance.

1.3 REPORT OUTLINE

The subsequent chapters of this report contain the following material: Chapter 2 is concerned with the development of the system model and the derivation of the extended and quasi-linear Kalman filter algorithms, Chapter 3 deals with direct performance comparisons of the two types of algorithms in a few key situations, and Chapter 4 presents a summary of the investigation and the conclusions derived from the study. Appendix A provides an overview of nonlinear estimation theory, and Appendix B treats the evaluation of random-input describing functions for the arctangent nonlinearity involved in the bearing measurement equation.

2. MODEL DEVELOPMENT

In this chapter, the range estimation problem under investigation is specified by deriving a simple mathematical model to represent the missile and target dynamics. One essential nonlinear effect is incorporated: the LOS angle measurement relation (Eq. (1.1-1)). The model described here is quite similar to that of Ref. 1; the problem has been simplified, however, by the exclusion of some secondary error sources (altimeter bias and random altitude measurement error, accelerometer bias, attitude reference tilt and gyro drift). The elimination of these error sources does not compromise the degree of realism necessary to achieve the goals of the study.

2.1 TARGET MOTION MODEL

The range estimation problem outlined in Section 1.1 deals with the planar intercept case, with the motion of the target constrained to be along the horizontal or x axis (Fig. 1.1-1). We assume that the target acceleration magnitude, a_t, is a first-order Markov process, modeled as a zero-mean gaussian white noise process, w, passed through a single stage of low-pass filtering, as depicted in Fig. 2.1-1. By suitably adjusting the values of the target maneuver bandwidth, ω_t, and acceleration rms level, σ_a, a wide variety of random target maneuvers can be realistically represented. A constant rms level of horizontal acceleration is assumed for the present study,*

*E[] denotes the expected value of the bracketed variable.

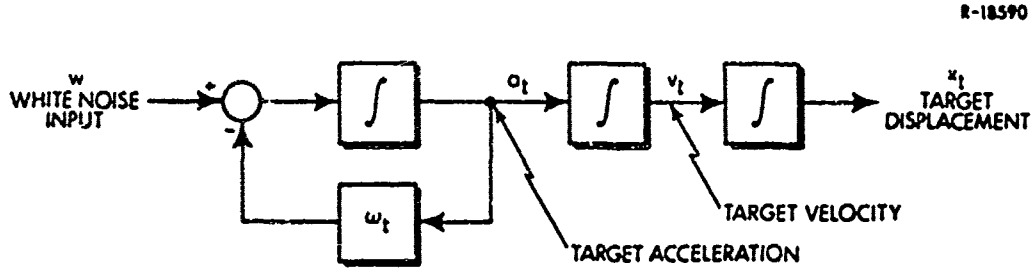

Figure 2.1-1 Target Maneuver Model

$$E\left[a_t^2(t)\right] \equiv \sigma_{a_o}^2 \qquad (2.1\text{-}1)$$

To achieve this condition, the spectral density of the white noise process, q, is specified by

$$E\left[w(t)w(\tau)\right] \triangleq q\ \delta(t-\tau) = 2\omega_t \sigma_{a_o}^2\ \delta(t-\tau) \qquad (2.1\text{-}2)$$

A ship of moderate maneuverability can be modeled by choosing the bandwidth and rms acceleration level to be 0.05 rad/sec and 3.22 ft/sec^2 (0.1g), respectively. The target horizontal velocity and position in an earth-fixed inertial frame, v_t and x_t respectively, are then obtained by integration (Fig. 2.1-1)

2.2 MISSILE TRAJECTORY GENERATOR

The motion of the missile with respect to an earth-fixed inertial frame is modeled deterministically by a trajectory generator that produces a specified time history of missile position, x_m and y_m, missile velocity, v_{m_x} and v_{m_y}, and missile acceleration, a_{m_x} and a_{m_y}, in Cartesian coordinates. By utilizing the specified trajectory, the need for modeling the guidance and control system is avoided.

Furthermore, by removing the range estimation function from the guidance and control loop, it is guaranteed that the same trajectory will be followed in each case studied, making the filter performance evaluations exactly comparable.

The trajectory is qualitatively similar to that portrayed in Fig. 1.1-1, i.e., there is an initial low-altitude cruise phase of 7.2 sec followed by a pitch-up terminal maneuver. Details of the trajectory, expressed in normalized units, are given in Chapter 3.

2.3 STATE VECTOR DIFFERENTIAL EQUATION AND MEASUREMENT MODEL

The five state variables used in the missile-target ranging problem are indicated in Table 2.3-1. Observe that the horizontal separation and separation rate are relative, i.e., the state variables x_1 and x_2 represent the horizontal displacement and velocity from the missile to the target. The state vector differential equation then has one random input w (Fig. 2.1-1) and two deterministic or known inputs, a_{m_x} and a_{m_y}, which are henceforth denoted by u_1 and u_2, respectively. By considering the missile accelerations to be deterministic filter inputs, it is assumed that errors that may arise in the resolved body-mounted accelerometer measurements are negligible in comparison with the LOS angle measurement errors. In terms of the above variables, the relative missile-target motion is governed by

$$\dot{\underline{x}} = F\underline{x} + \underline{g}w + L\underline{u} \qquad (2.3\text{-}1)$$

TABLE 2.3-1

STATE VARIABLES IN THE MISSILE-TARGET RANGE ESTIMATION PROBLEM

STATE VARIABLE	ALTERNATIVE SYMBOL	INTERPRETATION
x_1	$x_m - x_t$	Missile-target horizontal separation
x_2	$v_{m_x} - v_t$	Missile-target horizontal separation rate
x_3	y_m	Missile altitude
x_4	v_{m_y}	Missile altitude rate
x_5	a_t	Target horizontal acceleration

where

$$F = \begin{bmatrix} 0 & 1 & 0 & 0 & 0 \\ 0 & 0 & 0 & 0 & -1 \\ 0 & 0 & 0 & 1 & 0 \\ 0 & 0 & 0 & 0 & 0 \\ 0 & 0 & 0 & 0 & -\omega_t \end{bmatrix} , \quad \underline{g} = \begin{bmatrix} 0 \\ 0 \\ 0 \\ 0 \\ 1 \end{bmatrix} , \quad L = \begin{bmatrix} 0 & 0 \\ 1 & 0 \\ 0 & 0 \\ 0 & 1 \\ 0 & 0 \end{bmatrix} \tag{2.3-2}$$

The scalar measurement available for range estimation is a corrupted observation of line-of-sight angle sampled at times t_k,

$$\begin{aligned} z_k &= \tan^{-1}(x_3(t_k)/x_1(t_k)) + v_k \\ &\triangleq \theta_k + v_k , \quad k = 0,1,2,\ldots \end{aligned} \tag{2.3-3}$$

where it is assumed that the sampling rate is uniform,

$$t_k = k\tau \tag{2.3-4}$$

with sampling interval, τ. The measurement noise sequence v_k is assumed to be a zero-mean gaussian random process with

constant variance ρ_v,

$$\begin{aligned} E[v_k] &= 0 \\ & \quad , \quad k = 0,1,2,\ldots \\ E[v_k^2] &= \rho_v \end{aligned} \tag{2.3-5}$$

A further source of measurement inaccuracy considered in this investigation is quantization, which is denoted by the nonlinear operation $f_q(\cdot)$ defined by

$$f_q(z) = \begin{cases} 0 \quad , & |z| < \delta/2 \\ \delta \text{ sign } z \ , & \delta/2 \le |z| < 3\delta/2 \\ 2\delta \text{ sign } z, & 3\delta/2 \le |z| < 5\delta/2 \\ \quad \vdots & \quad \vdots \\ N\delta \text{ sign } z, & (2N-1)\delta/2 \le |z| < \infty \end{cases} \tag{2.3-6}$$

The quantizer output takes on the (2N+1) discrete values $0, \pm\delta, \pm 2\delta, \ldots, \pm N\delta$ as z varies continuously. It is assumed that quantization occurs after the corruption of the LOS angle measurement by the random sequence v_k,

$$z_{q,k} = f_q\left\{\tan^{-1}(x_3(t_k)/x_1(t_k)) + v_k\right\} \tag{2.3-7}$$

This last relation is the most general measurement equation considered in this study.

An overview of the system dynamics and measurement model is provided in Fig. 2.3-1. This model serves as the basis for the design of filter algorithms to estimate target position, velocity and acceleration when the only available measurement of relative target position is LOS angle.

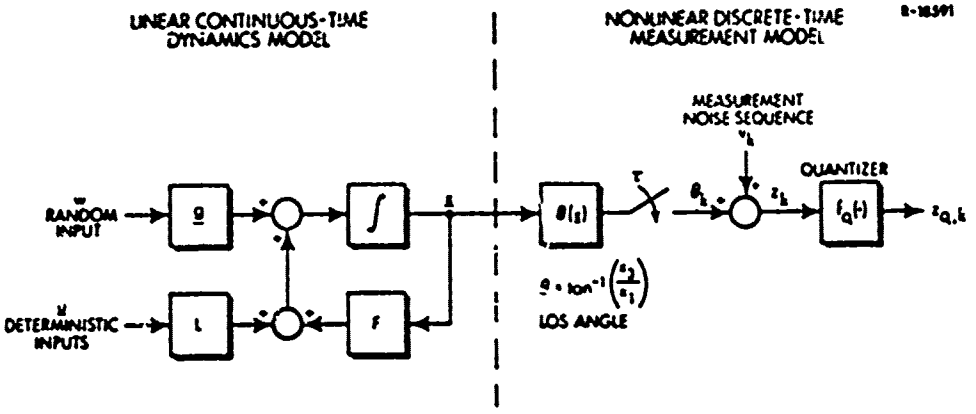

Figure 2.3-1 Mathematical Model for the Range Estimation Problem

2.4 LINEARIZED MEASUREMENT MODELS AND MODIFIED KALMAN FILTER ALGORITHMS

2.4.1 Filter Algorithms When Quantization is Absent

Equations (2.3-1) to (2.3-3) provide the basis for designing both the extended Kalman filter (EKF) and quasi-linear Kalman filter (QKF) for the range estimation problem when quantization is not present. The system dynamics, indicated in Eq. (2.3-1), are linear, so it is necessary to linearize only the measurement, Eq. (2.3-3). Two approaches are used in this study.

The first technique considered is small-signal linearization about the current filter estimate of the state,

$$z_{S,k} = \tan^{-1}(\hat{x}_3/\hat{x}_1) + \frac{\partial}{\partial x_1}\tan^{-1}\left(\frac{x_3}{x_1}\right)\Bigg|_{\underline{x}=\hat{\underline{x}}}(x_1-\hat{x}_1)$$

$$+ \frac{\partial}{\partial x_3}\tan^{-1}\left(\frac{x_3}{x_1}\right)\Bigg|_{\underline{x}=\hat{\underline{x}}}(x_3-\hat{x}_3) + v_k$$

$$\triangleq \theta(\hat{\underline{x}}) + \underline{h}_S^T\,\tilde{\underline{x}} + v_k \qquad (2.4\text{-}1)$$

The vector $\underline{h}_S$ is given by

$$\underline{h}_S^T = \left[\frac{\partial}{\partial x_1} \tan^{-1}\left(\frac{x_3}{x_1}\right)\Bigg|_{\underline{x}=\hat{\underline{x}}} \quad 0 \quad \frac{\partial}{\partial x_3} \tan^{-1}\left(\frac{x_3}{x_1}\right)\Bigg|_{\underline{x}=\hat{\underline{x}}} \quad 0 \quad 0 \right] \tag{2.4-2}$$

and $\tilde{\underline{x}} \triangleq \underline{x} - \hat{\underline{x}}$ is the difference between the true state vector and the current estimate.

The second linearization technique is called quasi-linearization (Ref. 3); it entails replacing Eq. (2.3-3) with the random-input describing function (ridf) representation

$$z_{Q,k} = \hat{\theta} + \underline{h}_Q^T \tilde{\underline{x}} + v_k \tag{2.4-3}$$

In this approximation, $\hat{\theta}$ and $\underline{h}_Q$ are given by

$$\hat{\theta} \triangleq E\left[\tan^{-1}(x_3/x_1)\right]$$

$$\underline{h}_Q^T \triangleq E\left[\tilde{\underline{x}}^T \tan^{-1}(x_3/x_1)\right] P^{-1} \tag{2.4-4}$$

where E[ ] denotes expected value, $\tilde{\underline{x}}$ is the random part of $\underline{x}$,

$$\tilde{\underline{x}} \triangleq \underline{x} - E[\underline{x}]$$

and P is the associated covariance matrix,

$$P \triangleq E[\tilde{\underline{x}}\ \tilde{\underline{x}}^T]$$

The quantities $\hat{\theta}$, $\underline{h}_Q$ defined in Eq. (2.4-4) satisfy the condition that the resulting mean square error in approximating Eq. (2.3-3) by Eq. (2.4-3) is minimized.

In the standard ridf methodology, the expected values indicated in Eq. (2.4-4) are evaluated by assuming that $\underline{x}$ is a vector of gaussian random variables with mean $\underline{m}$ and covariance matrix P. In the present application, $\underline{m}$ is the current state estimate, $\hat{\underline{x}}$, and P is the filter covariance matrix which is propagated as part of the recursive algorithm detailed subsequently. As noted in Appendix A, the gaussian assumption results in the dependence of the ridf's on $\hat{\underline{x}}$ and P alone:

$$\hat{\theta}_k = \hat{\theta}_k(\hat{\underline{x}}, P)$$

$$\underline{h}_Q = \underline{h}_Q(\hat{\underline{x}}, P)$$

In the studies described in Chapter 3, three distinct quasi-linear representations of arctan (y/x) are considered. One reason for this multiplicity is that $\hat{\theta}$ and $\underline{h}_Q$ defined as in Eq. (2.4-4) cannot be evaluated analytically in closed form when x and y are jointly normal; consequently two approximate techniques have been applied to the problem. The third ridf model for this nonlinearity is based on a nongaussian density function; it was developed to study the impact of the gaussian assumption on the performance of a quasi-linear Kalman filter (QKF) algorithm.

The most accurate gaussian-based ridf is obtained by numerical integration; the filter which utilizes that approach is designated the QKF-N and the ridf components are denoted $\hat{\theta}_N$, $\underline{h}_{Q_N}$. A simpler ridf representation of arctan (y/x) is obtained by a power series expansion technique; it should be noted that this leads to ridf's that are distribution independent. The corresponding filter algorithm and ridf components are called the QKF-P and $\hat{\theta}_P$, h_{Q_P}, respectively. The third quasi-linear representation is based on a truncated and folded gaussian density,

$$p_T(x,y) = \begin{cases} 0 & , x < 0 \\ p(x,y) + p(-x,y) & , x \geq 0 \end{cases} \qquad (2.4\text{-}5)$$

where $p(x,y)$ is the joint density of x and y under the gaussian assumption (cf. Eq. (B.1-5)); by truncating the density at $x = 0$, it is assumed that there is no probability that the missile has flown past the ship. Using the truncated density, Eq. (2.4-5), numerical integration is used to obtain $\hat{\theta}_T$, $\underline{h}_{Q_T}$; substituting these results in the quasi-linear filter algorithm leads to the QKF-T. Details concerning the evaluation of these ridf's are given in Appendix B.

The above linearized measurement models are nearly the same when the estimation error variances (elements of P) are small. However, if there is significant uncertainty in the estimate, they differ considerably. The comparison indicated in Table 2.4-1, normalized to a unity altitude estimate,

TABLE 2.4-1

COMPARISON OF SMALL-SIGNAL LINEAR AND QUASI-LINEAR APPROXIMATIONS OF ARCTAN $(\hat{x}_3/\hat{x}_1)$*

Estimates and Estimation Error Variances	$\hat{x}_1$ = 40.0 units $\hat{x}_3$ = 1.0 units	p_{11} = (20.0 units)^2 p_{13} = 0.0 p_{33} = (0.2 units)^2	
Linearization Technique	$\theta(\hat{x})$ or $\hat{\theta}$(rad)	h_1(rad/unit)	h_3(rad/unit)
Small-Signal	2.5×10^{-2}	-1.25×10^{-5}	5.00×10^{-4}
Quasi-Linear, Numerical Integration	1.00×10^{-1}	-1.79×10^{-4}	8.25×10^{-4}
Quasi-Linear, Power Series	3.12×10^{-2}	-2.19×10^{-5}	6.24×10^{-4}
Quasi-Linear, Truncated Density	4.08×10^{-2}	-2.95×10^{-5}	8.93×10^{-4}

*"unit" denotes a normalized length, p_{ij} are the relevant entries of P, and h_1, h_3 are the nonzero elements of $\underline{h}_S$ or $\underline{h}_Q$.

$\hat{x}_3 = 1$, indicates that a 50 percent uncertainty in the horizontal separation estimate can lead to large disparities; these conditions may not be unreasonable during the cruise phase.

The extended Kalman filter (EKF) algorithm is mechanized according to the following relations: given $\underline{x}_{k-1}(+)$ and $P_{k-1}(+)$ as the state vector estimate and filter covariance matrix after the previous measurement and update, the filter variables satisfy

Extrapolation Between Measurements

$$\underline{\hat{x}}_k(-) = \Phi_\tau \underline{\hat{x}}_{k-1}(+) + \int_{t_{k-1}}^{t_k} \Phi(t_k - t) L\, \underline{u}(t)dt$$

$$P_k(-) = \Phi_\tau P_{k-1}(+)\Phi_\tau^T + Q_d \qquad (2.4\text{-}6)$$

where

$$\Phi(t) \triangleq \exp(Ft)$$

$$\Phi_\tau \triangleq \Phi(\tau)$$

$$Q_d \triangleq q\int_0^\tau \Phi(\tau-\xi)\, \underline{g}\underline{g}^T \Phi^T(\tau-\xi)d\xi \qquad (2.4\text{-}7)$$

and q is the spectral density of w (Eq.(2.1-2)),

Update at a Measurement

$$\underline{\hat{x}}_k(+) = \underline{\hat{x}}_k(-) + \underline{k}_k\left[z_k - \theta(\underline{\hat{x}}_k(-))\right]$$

$$P_k(+) = \left[I - \underline{k}_k \underline{h}_S^T(\underline{\hat{x}}_k(-))\right] P_k(-) \qquad (2.4\text{-}8)$$

where

$$\underline{k}_k \triangleq P_k(-)\underline{h}_S/(\underline{h}_S^T P_k(-)\underline{h}_S + \rho_v) \qquad (2.4\text{-}9)$$

The first step of the above procedure, Eq. (2.4-6), propagates the filter estimate over the time period between measurements, according to the linear dynamic model of Eqs. (2.3-1) and (2.3-2), and the modification of P reflects the change in estimation error covariance during the same interval. The second step, Eq. (2.4-8), represents the use of the current measurement z_k to update the state vector estimate. The auxiliary matrices indicated in Eqs. (2.4-7) and (2.4-9) are the general transition matrix, $\Phi(t)$, the transition matrix evaluated over one sample time, Φ_τ, the equivalent discrete noise matrix, Q_d, and the Kalman gain vector, $\underline{k}_k$. Equations (2.4-6) to (2.4-9) are the particular case of the EKF algorithm presented in Appendix A.

The quasi-linear Kalman filter (QKF) for the present problem differs from the above EKF algorithm only in tne update step:

$$\begin{aligned} \hat{\underline{x}}_k(+) &= \hat{\underline{x}}_k(-) + \underline{k}_k\left[z_k - \hat{\theta}(\hat{\underline{x}}_k(-), P_k(-))\right] \\ P_k(+) &= \left[I - \underline{k}_k \underline{h}_Q^T(\hat{\underline{x}}_k(-), P_k(-))\right] P_k(-) \end{aligned} \tag{2.4-10}$$

where

$$\underline{k}_k \triangleq P_k(-)\underline{h}_Q / (\underline{h}_Q^T P_k(-)\underline{h}_Q + \rho_v) \tag{2.4-11}$$

The extrapolation step is unchanged, since the system dynamics equations are linear. These equations are considered in more detail in Section A.3.

2.4.2 Filter Algorithms When Quantization is Present

Introduction of the quantization nonlinearity $f_q(\cdot)$ given in Eq. (2.3-6) in the measurement, as in Eq. (2.3-7),

requires further modification of the estimation algorithms given in Section 2.4.1. The approaches used to deal with this effect in the EKF and QKF algorithms are quite different, since the discontinuous nature of the nonlinearity precludes the formal use of small signal linearization, as mentioned in Section A.2.

Observe that the quantizer characteristic in Eq. (2.3-6) approaches a continuous linear unity gain characteristic as δ goes to zero and N goes to infinity. This implies that quantization can be ignored in the limit as the cell-width δ becomes small. and we can replace the quantizer with a unity gain. When δ is not infinitesimal, it is clearly not reasonable to make a formal application of the EKF principle of small-signal linearization,

$$h(\underline{x}) \cong h(\underline{\hat{x}}) + \frac{\partial h}{\partial \underline{x}}\bigg|_{\substack{\underline{\tilde{x}} \\ \underline{x}=\underline{\hat{x}}}}$$

$$\triangleq h(\underline{\hat{x}}) + \underline{h}_S^T \underline{\tilde{x}}$$

since the fact that the nonlinearity has zero slope for almost all values of the input would lead to setting $\underline{h}_S$ to be zero. A more intuitively satisfactory linearization technique entails replacing the quantizer with a unity gain (Ref. 4) and modeling the difference between the input and the output as an additive white quantization noise, v_q. If the quantizer input probability density function is nearly constant over each cell, then it is accurate to assume that v_q is uniformly distributed over the interval $-\frac{1}{2}\delta$, $\frac{1}{2}\delta$. As can readily be established (cf. Table C.2-1 of Ref. 5), a random variable with this distribution has a zero mean and rms level of $\delta/\sqrt{12}$. If this artificial random process is assumed to be uncorrelated with the real

measurement noise sequence v_k in Eq. (2.3-3), the total measurement noise variance is then

$$\rho_q = \rho_v + \delta^2/12 \tag{2.4-12}$$

Modifying the measurement noise variance as in Eq. (2.4-12) completely accounts for the effect of quantization in the small-signal linearized measurement model.

A quasi-linear model for the quantization effect defined in Eq. (2.3-6) is needed for the QKF. Given the input statistics,

$$E[z] = m$$
$$E[(z-m)^2] = \sigma^2$$

the quasi-linear representation of the quantizer is of the form

$$f_q(z) \cong \hat{f}_q(m,\sigma) + n_q(m,\sigma)(z-m) \tag{2.4-13}$$

The ridf's indicated in Eq. (2.4-14) are (Ref. 3)

$$\hat{f}_q = \delta \sum_{i=1}^{N} \left[PI\left(\frac{(2i-1)\delta}{2\sigma} + \frac{m}{\sigma}\right) - PI\left(\frac{(2i-1)\delta}{2\sigma} - \frac{m}{\sigma}\right)\right]$$
$$n_q = \frac{\delta}{\sigma} \sum_{i=1}^{N} \left[PF\left(\frac{(2i-1)\delta}{2\sigma} + \frac{m}{\sigma}\right) + PF\left(\frac{(2i-1)\delta}{2\sigma} - \frac{m}{\sigma}\right)\right] \tag{2.4-15}$$

where

$$PF(v) = \frac{1}{\sqrt{2\pi}} e^{-\frac{1}{2}v^2}$$
$$PI(v) = \int_{-\infty}^{v} PF(\nu)d\nu \tag{2.4-16}$$

From the quasi-linear representation of the noisy LOS angle measurement before quantization, $z_{Q,k}$ (Eq. (2.4-3)), the quantizer input statistics are evaluated approximately as

$$\begin{aligned} m &= \hat{\theta} \\ \sigma^2 &\cong \underline{h}_Q^T P \underline{h}_Q + \rho_v \end{aligned} \tag{2.4-17}$$

The complete quasi-linear measurement model is then obtained by cascading the random component ridf's as follows:

$$z_{q_{Q,k}} = \hat{f}_q + n_q(\underline{h}_Q^T \tilde{\underline{x}} + v_k) \tag{2.4-18}$$

The two linearized measurement models described above are depicted in Fig. 2.4-1. In the small signal or EKF case, the addition of the fictitious quantization noise (Eq. (2.4-12)) to the model given in Eq. (2.4-1) completely accounts for the quantizer, while the quasi-linear representation of the same effect introduces a describing function gain, n_q, and a modified expected value, $\hat{f}_q$.

On the basis of the above arguments, the EKF algorithm modification that accounts for the presence of LOS angle quantization is obtained by merely replacing ρ_v in Eq. (2.4-9) with ρ_q given in Eq. (2.4-12),

$$\underline{k}_k = P_k(-)\underline{h}_S/(\underline{h}_S^T P_k(-)\underline{h}_S + \rho_v + \delta^2/12) \tag{2.4-19}$$

The quasi-linear model of Eq. (2.4-18) is seen to result in the QKF algorithm having measurement update equations of the form

$$\begin{aligned} \hat{\underline{x}}_k(+) &= \hat{\underline{x}}_k(-) + \underline{k}_k(z_k - f_q(m,\sigma)) \\ P_k(+) &= \left[I - n_q(m,\sigma)\underline{k}_k \underline{h}_Q^T(\hat{\underline{x}}_k(-), P_k(-))\right] P_k(-) \end{aligned} \tag{2.4-20}$$

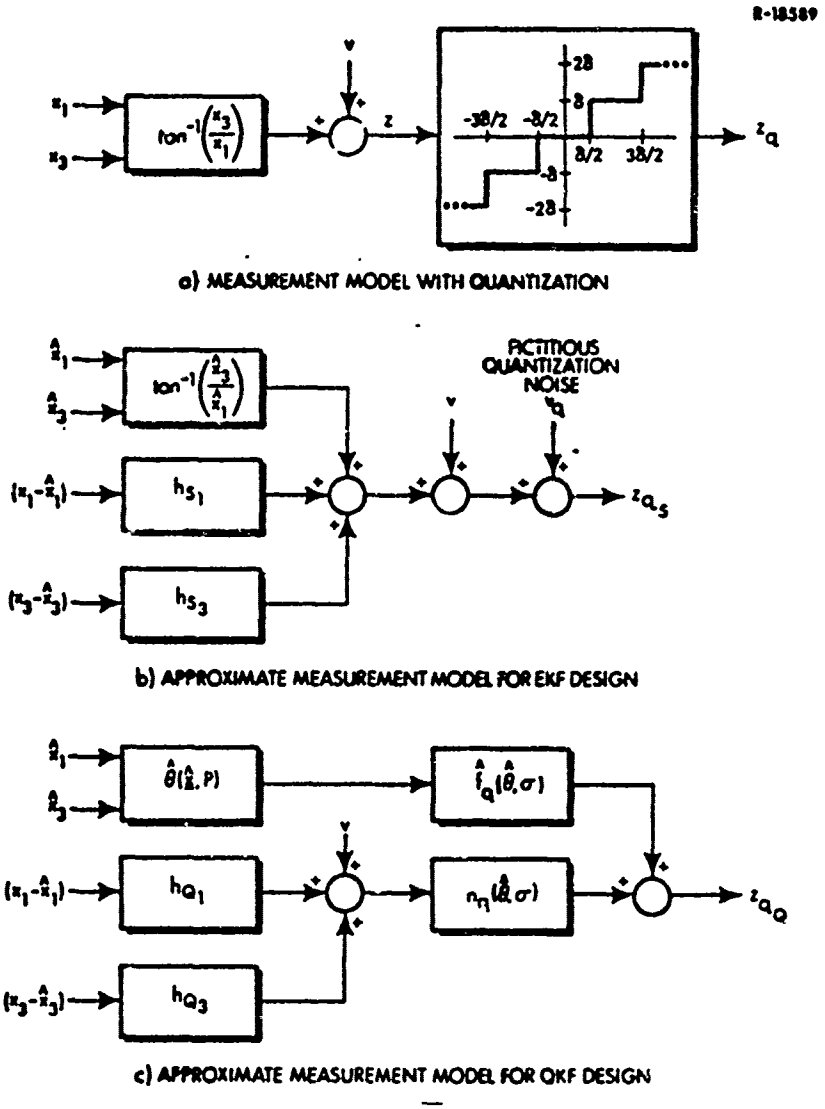

Figure 2.4-1 LOS Angle Measurement Quantization Models

where

$$\underline{k}_k = P_k(-)\underline{h}_Q\left(\hat{\underline{x}}_k(-), P_k(-)\right) \Big/ \left(n_q(m,\sigma)\left[\underline{h}_Q^T P_k(-)\underline{h}_Q + \rho_v\right]\right) \quad (2.4\text{-}21)$$

The algorithms given in this section for estimating relative missile-target position, velocity and acceleration are based on two quite general and powerful nonlinear

estimation techniques: the extended Kalman filter (EKF) and the quasi-linear Kalman filter (QKF). The goal of this study is to determine their performance (both absolute and comparative) in the antishipping missile application (Fig. 1.1-1).

3. FILTER RANGE ESTIMATION PERFORMANCE

3.1 PRELIMINARIES

The missile from which the target line-of-sight angle (LOS angle) measurements are taken follows a deterministic trajectory which is qualitatively depicted in Fig. 1.1-1. The initial 7.2 sec of the flight is a constant-altitude cruise, with normalized altitude of unity (y=1 unit) and an initial horizontal missile-target separation, x_o, of 425 units. The cruise phase of the engagement ends at x=300 units and is followed by a pitch-up maneuver. The latter leads to a maximum altitude of about 22 units at 19 sec and terminates at the nominal target position at 26.5 sec. It is assumed that the motion of the target is characterized by a horizontal acceleration which is a zero-mean correlated gaussian random process with bandwidth 0.05 rad/sec and rms level of 3.22 ft/sec^2; these parameter values are representative of a moderately large ship conducting a slow random maneuver. The LOS angle measurement noise sequence, v_k in Eq. (2.3-3), is always assumed to be a zero-mean discrete gaussian process with rms level 4.38 mrad (0.25 deg); the data rate is 5 measurements/sec.

In order to assess the performance of the various filter algorithms, a single random realization of the stochastic nonlinear estimation problem is obtained. Random number generators are used to generate a suitable measurement noise sequence, v_k, and random target acceleration sample function, a_t. In all of the engagements presented here, the time-histories of v_k and a_t are the same,

which permits direct comparison. The variables of greatest concern are the initial values of the error in the filter estimates, $\underline{x}_0$, and the uncertainty of these estimates, P_0, whe

$$\begin{aligned} \tilde{\underline{x}}_0 &\triangleq \underline{x}(0) - \hat{\underline{x}}(0) \\ P_0 &= E\left[\tilde{\underline{x}}_0 \tilde{\underline{x}}_0^T\right] \end{aligned} \tag{3.1-1}$$

The initial state vector is always specified by*

$$\underline{x}(0) = \begin{bmatrix} 425.3 & u \\ -17.90 & u/sec \\ 1.0 & u \\ 0.0 & u/sec \\ 6.142 & ft/sec^2 \end{bmatrix} \tag{3.1-2}$$

The initial estimation error covariance matrix is assumed to be of the form

$$P_0 \triangleq \begin{bmatrix} \sigma_{x_0}^2 & \rho\sigma_{x_0}\sigma_{\dot{x}_0} & 0 & 0 & 0 \\ \rho\sigma_{x_0}\sigma_{\dot{x}_0} & \sigma_{\dot{x}_0}^2 & 0 & 0 & 0 \\ 0 & 0 & \sigma_{y_0}^2 & \rho\sigma_{y_0}\sigma_{\dot{y}_0} & 0 \\ 0 & 0 & \rho\sigma_{y_0}\sigma_{\dot{y}_0} & \sigma_{\dot{y}_0}^2 & 0 \\ 0 & 0 & 0 & 0 & \sigma_{a_0}^2 \end{bmatrix} \tag{3.1-3}$$

where ρ is chosen to be 0.707, which allows for correlation between the initial velocity and position estimates, in each

*The abbreviation u stands for unit (normalized length).

coordinate. Thus, P_0 is completely specified by the five diagonal elements, or their square roots. For convenient reference, the vector $\underline{\sigma}_0$ is defined as follows,

$$\sigma_0^T \triangleq \left[\sigma_{x_0} \; \sigma_{\dot{x}_0} \; \sigma_{y_0} \; \sigma_{\dot{y}_0} \; \sigma_{a_0}\right] \tag{3.1-4}$$

Finally, the error, $\tilde{r}$, in estimated range, and the estimate of rms range uncertainty,* σ_r, provided by the filter covariance matrix are of particular interest; these are given by

$$\begin{aligned}
\tilde{r} &\triangleq r - \hat{r} \\
&= \sqrt{x^2+y^2} - \sqrt{\hat{x}^2+\hat{y}^2} \\
\sigma_r &\cong \left[\left(\frac{\partial r}{\partial \underline{x}}\right)^T P \frac{\partial r}{\partial \underline{x}}\right]^{\frac{1}{2}} \\
&= \left[(p_{11}\hat{x}^2 + 2p_{13}\hat{x}\hat{y} + p_{33}\hat{y}^2)/(\hat{x}^2+\hat{y}^2)\right]^{\frac{1}{2}}
\end{aligned} \tag{3.1-5}$$

3.2 MEASUREMENT WITHOUT QUANTIZATION

The filter performance comparisons presented in this section are for situations where quantization effects can be neglected. The engagements investigated are categorized according to the assumed value of the initial rms horizontal-separation estimation error, σ_{x_0}.

*Note that σ_r is not the true rms range estimation error because the filter covariance matrix is generally not equal to the actual estimation error covariance in a nonlinear filtering problem.

3.2.1 Small Initial rms Horizontal-Separation Estimation Error

The initial values of $\underline{\tilde{x}}$ and $\underline{\sigma}$ are specified by

$$\underline{\tilde{x}}_0 = \begin{bmatrix} -4.67 & u \\ 0.703 & u/sec \\ 0.2 & u \\ -0.08 & u/sec \\ 6.142 & ft/sec^2 \end{bmatrix}, \quad \underline{\sigma}_0 = \begin{bmatrix} 4.29 & u \\ 0.707 & u/sec \\ 0.209 & u \\ 0.0849 & u/sec \\ 3.22 & ft/sec^2 \end{bmatrix} \qquad (3.2\text{-}1)$$

These conditions correspond closely to the nominal case of Ref. 1 without altimeter measurements; they are typical of situations where radar range measurements are available until the filter initialization time, when they are denied by target jamming activity.

The time-histories of $\tilde{r}$, the range estimation error, and σ_r, the rms filter range uncertainty, are depicted in Fig. 3.2-1. Since σ_x is much smaller than $\hat{x}$ for the first 10 sec of the engagement,* it might be anticipated that the EKF and the two QKF algorithms should perform nearly identically, as is indicated in Fig. 3.2-1. In mid-engagement, however, there is some departure between the EKF and the QKF with accurate ridf's determined by numerical integration, denoted QKF-N (Sections 2.4 and B.3). Observe that the QKF with approximate ridf's based on a power series expansion (Section B.2), which is designated QKF-P, is indistinguishable from the EKF. The QKF based on the truncated gaussian density (QKF-T) was not exercised for this case; as shown

*Since the missile altitude is always much smaller than the horizontal missile-target separation, the pairs (x,r), (σ_x,σ_r) and $(\tilde{x},\tilde{r})$ are very nearly equal in the studies performed here.

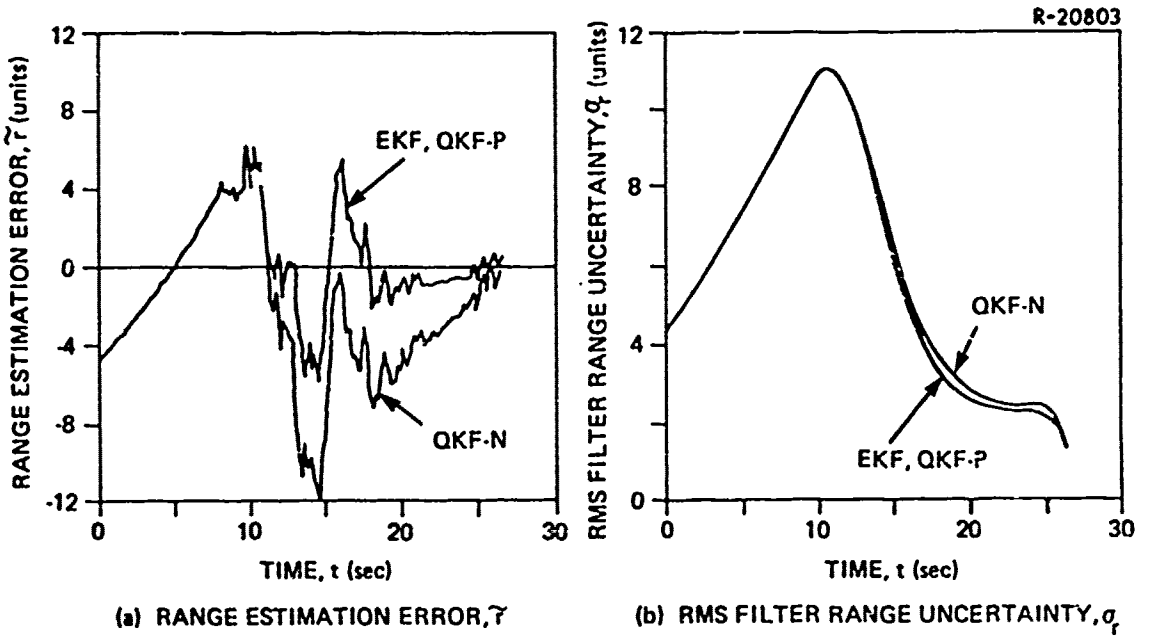

Figure 3.2-1 Time-Histories of Range Estimation Error and Uncertainty for Small Initial Uncertainty

subsequently, its performance can be anticipated to be intermediate to that of the QKF-N and the QKF-P.

The relative behavior of the three filter algorithms directly reflects the comparative values for the linearized measurement model parameters -- θ or $\hat{\theta}$, h_1, and h_3 -- listed in Table 2.4-1. The table demonstrates that corresponding values of these parameters are more nearly equal for the EKF (small-signal linearization) and the QKF-P (power series) than for either the EKF or the QKF-P and the QKF-N (numerical integration). All algorithms maintain σ_r and $\tilde{r}$ within the range ± 12 units for the trial performed, which may be adequate in some circumstances, especially in the first half of the engagement ($t<15$ sec) when range is greater than 180 units.

3.2.2 Large Initial rms Horizontal-Separation Estimation Error

The initial rms error in the horizontal separation estimate was increased to 220 units, to represent very poor filter initialization. Five initial values of $\tilde{x}_0$ were considered, viz., 225, 125, 25, -75 and -175 units, which are designated Cases 1 to 5, respectively. As mentioned previously, $\tilde{r}_0 \cong \tilde{x}_0$, since $\tilde{y}_0$ is small. Both the QKF-N and the EKF were exercised for all initializations; the truncated gaussian quasi-linear algorithm, QKF-T, was applied to Cases 1, 3 and 5, and the approximate QKF-P was evaluated for Cases 1 and 5. Figure 3.2-2 depicts the simulation results.

An adverse effect observed in the QKF-N time histories of $\tilde{r}$ is a large negative step change at the time the first measurement is processed, followed by a long period of relative inactivity; $\tilde{r}$ changes only slightly over the first ten seconds after the first filter update. The reason for this quiescent behavior is clearly evident in the corresponding plots of σ_r: The filter covariances become so small that subsequent Kalman gains are likewise very small, and thus the corresponding measurement data is virtually ignored. The small values of σ_r can be explained by contrasting the initial quasi-linear measurement equation parameters (QKF-N) with those obtained by small-signal linearization (EKF), as given in Table 3.2-1 for Case 1. Based on $\hat{x}_0$ and σ_{x_0}, the quasi-linear representation

$$\theta(x) \cong \hat{\theta}(\hat{x},P) + h_{Q_1}(x-\hat{x}) + h_{Q_3}(y-\hat{y})$$

gives rise to values of $\hat{\theta}$ and h_{Q_1} that are very large in comparison with the corresponding small-signal linearization

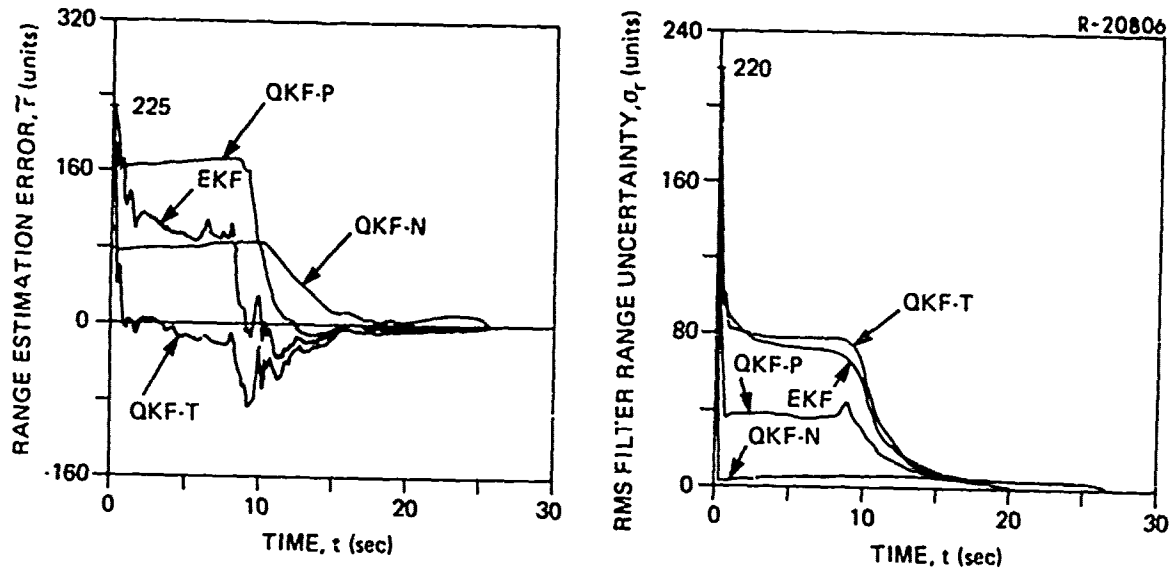

(a) FILTER PERFORMANCE CURVES FOR $\tilde{r}_0$ = 225 UNITS (CASE 1)

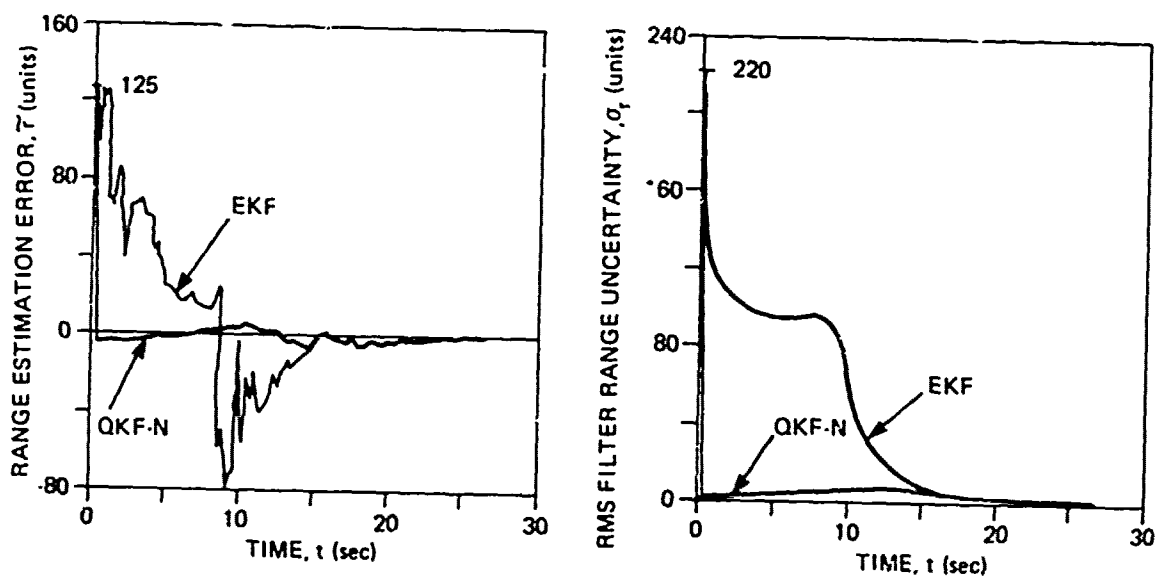

(b) FILTER PERFORMANCE CURVES FOR $\tilde{r}_0$ = 125 UNITS (CASE 2)

Figure 3.2-2 Time-Histories of Range Estimation Error and Uncertainty for Large Initial Uncertainty

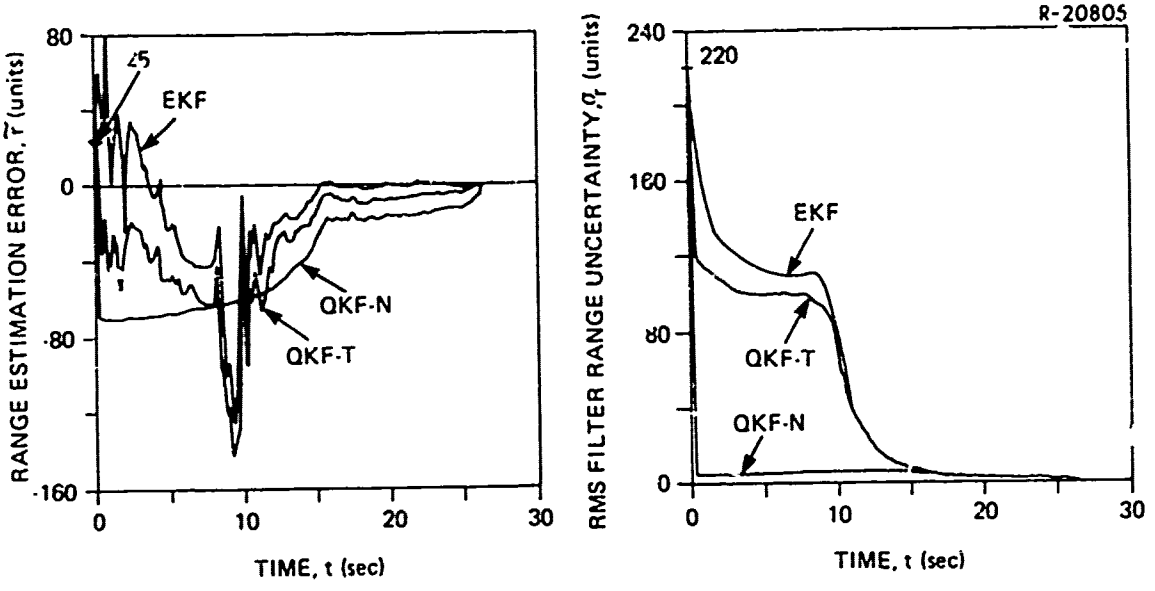

(c) FILTER PERFORMANCE CURVES FOR $\tilde{r}_0$ = 25 UNITS (CASE 3)

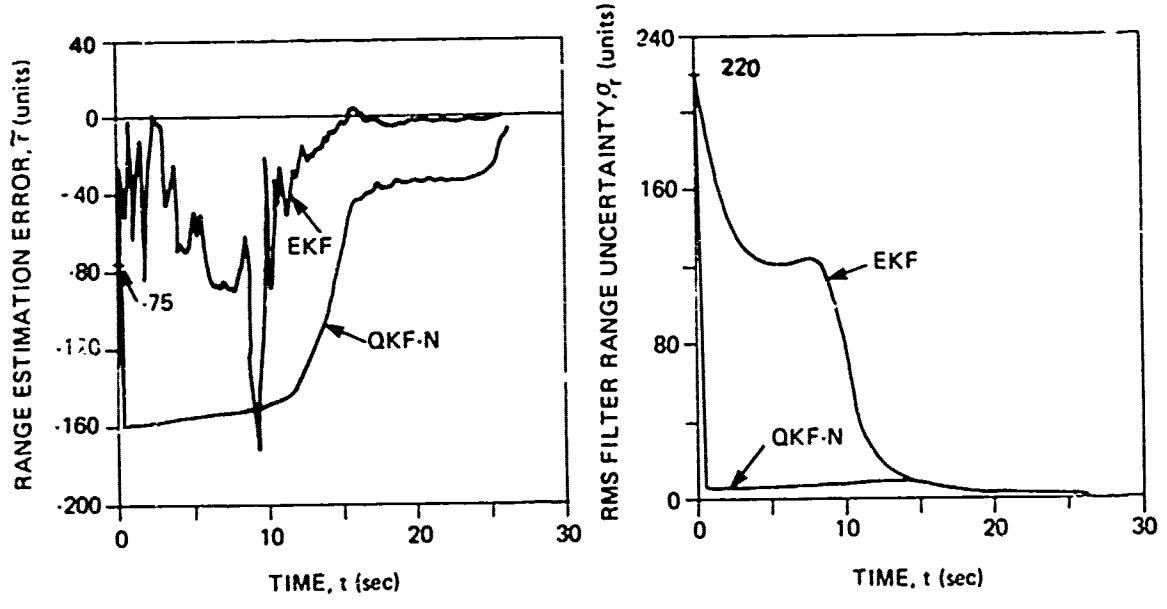

(d) FILTER PERFORMANCE CURVES FOR $\tilde{r}_0$ = -75 UNITS (CASE 4)

Figure 3.2-2 Time-Histories of Range Estimation Error and Uncertainty for Large Initial Uncertainty (Cont.)

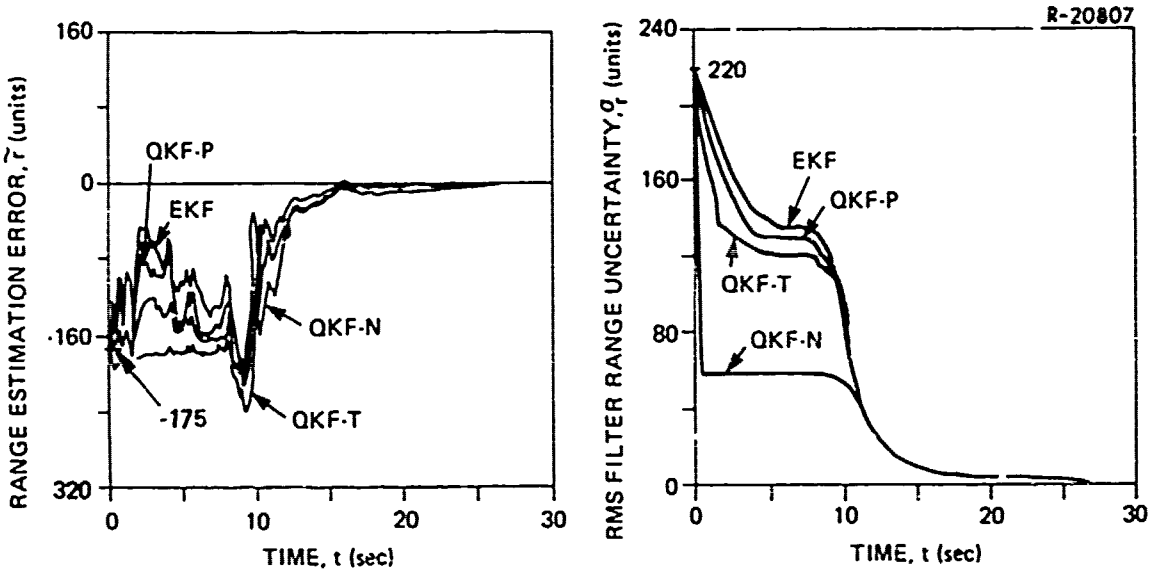

(e) FILTER PERFORMANCE CURVES FOR $\tilde{r}_0$ = -175 UNITS (CASE 5)

Figure 3.2-2 Time-Histories of Range Estimation Error and Uncertainty for Large Initial Uncertainty (Cont.)

TABLE 3.2-1

COMPARISON OF MEASUREMENT LINEARIZATION PARAMETERS, CASE 1

EKF	QKF-N
$\theta(\hat{\underline{x}}) = 0.00584$ rad	$\hat{\theta} = 0.573$ rad
$h_{S_1} = -6.31 \times 10^{-7}$	$h_{Q_1} = -7.72 \times 10^{-5}$
$h_{S_3} = 1.02 \times 10^{-4}$	$h_{Q_3} = 8.56 \times 10^{-5}$

parameters $\theta(\hat{x})$ and h_{S_1}. In the filter update equation for the QKF-N, Eq. (2.4-10), the large $\hat{\theta}$ and h_{Q_1} values result in a large change in $\hat{x}$ and in the (1,1) element of

$(I-\underline{k}_k \underline{h}_Q^T)$ being very small; this greatly reduces σ_x after the first update. The behavior of the QKF-N described above is clearly inappropriate in Cases 1,3,4 and 5; for Case 2, the apparent superiority of the QKF is "accidental," in that the large step change in $\tilde{r}$ just happens to be nearly "correct."

The QKF-P behaves somewhat like the QKF-N in Case 1. An abrupt initial change occurs in $\tilde{r}$, followed by small variations. Since σ_r for the QKF-P is larger than for the QKF-N, the QKF-P takes advantage of the additional angular information provided by the pitch-up maneuver sooner than the QKF-N, achieving a smaller value of $\tilde{r}$ after 10 sec. In Case 5, the QKF-P is much closer to the EKF in performance. This is attributed to the fact that $\hat{x}_0$ is much larger than σ_{x_0} for this case (by a factor of 3), resulting in a smaller difference between quasi-linearization (particularly in the power series approximation) and small-signal linearization, as shown in Fig. B.3-2.

The QKF-T was considered in this study to investigate the impact of using alternative densities for x. The truncated gaussian density, Eq. (2.4-5), was used in the numerical integration arctangent describing function subroutine (Section B.3) as the basis for describing function evaluations. It appears that the truncation of the density improves the QKF significantly for large positive initial range estimation errors (Fig. 3.2-2a), but that performance for small or large negative values of the initial estimation error is not better than the EKF in the same circumstances. Thus, while modifying the density function $p(\underline{x})$ upon which the quasi-linear filter is based does remove one deficiency of the gaussian-based QKF -- the large initial step change in r and ensuing 10 sec period of quiescent behavior discussed

above -- it does not appear that the QKF methodology is significantly superior to the simpler EKF algorithm in this application.

All filter algorithms appear to be more effective for $\tilde{r}>0$, i.e. for initial filter estimates of range that are smaller than the actual value. This result can be explained by the geometry of the situation: The arctangent nonlinearity and its slope become very small as $\hat{x}$ increases, which implies that it becomes more difficult to distinguish negative horizontal-separation estimation errors ($x<\hat{x}$) than positive ones of the same magnitude.

Of the algorithms considered, the QKF-N is the least effective, especially during the cruise phase. This is attributed to unrealistically small values of σ_x (or, equivalently, small values of σ_r -- Fig. 3.2-2) after the first measurement is processed. Considering the remaining filters, there does not appear to be a clear-cut advantage to any single algorithm. The EKF appears to have a bandwidth that is too wide, as may be deduced from the presence of large error "spikes" (at $t = 9$ sec, for example). The QKF-T and the approximate QKF-P are in some senses compromises between the EKF and the QKF-N (refer to Figs. 3.2-2 and B.3-2); they do not seem to offer any compelling advantages over the EKF for the cases studied, however. Because of the divergence for small values of $\hat{x}$ exhibited by the power series quasi-linear term, $\hat{\theta}_p$ (shown in Fig. B.3-2), it might be inadvisable to use the QKF-P design.

3.2.3 The Cramér-Rao Inequality

The studies discussed in Sections 3.2.1 and 3.2.2 indicate that the QKF methodology is not significantly superior to the EKF in the present application. This result was not anticipated since quasi-linearization generally provides a more realistic representation of a nonlinear effect than small-signal linearization, which should result in obtaining a more effective filter algorithm. However, there is a clear-cut explanation for the unexpected results in this investigation: The EKF appears to be quite effective in comparison with the "best that can be done" in the situation considered.

The Cramér-Rao inequality (Ref. 7) provides an absolute reference for judging the performance of a filter algorithm in solving a nonlinear estimation problem. Based on the system and measurement models, and on the initial statistics of the estimation error, this inequality provides a lower bound on the rms estimation error that is the best that can be achieved by any algorithm. In general terms, if $\hat{x}(z)$ is an unbiased estimate of the quantity x, which is based on a noisy measurement, z, then a fairly straightforward application of the Schwarz inequality leads to a lower bound on the variance of the estimation error,

$$E[(\hat{x}(z)-x)^2] \geq 1/E[(\partial \ln p(z|x)/\partial x)^2]$$

The function $p(z|x)$ is the conditional probability density function (pdf),

$$p(z|x) = p(x,z)/p(x)$$

where $p(x)$ and $p(x,z)$ are the pdf of x and the joint pdf of x and z, respectively. The Cramér-Rao inequality is useful for determining whether a given algorithm is comparable in

performance to the unspecified optimal algorithm, and thus, whether it is fruitful to attempt to design a "more sophisticated" filter for the same problem.

The result shown in Fig. 3.2-3 demonstrates the application of the Cramér-Rao lower bound to a scenario that is similar to, but slightly simpler than, the engagement studied in Section 3.2.2. P_0 in Eq. (3.1-3) is specified by setting the correlation coefficient ρ to zero and choosing $\underline{\sigma}_0$ to be

$$\underline{\sigma}_0 = \begin{bmatrix} 220.0 & u \\ 0.707 & u/sec \\ 0.209 & u \\ 0.0 & u/sec \\ 0.0 & ft/sec^2 \end{bmatrix}$$

Thus the target acceleration and altitude rate rms levels are neglected in this case. Furthermore, since range estimation in the cruise phase is of particular interest, the pitch-up missile maneuver is suppressed; the altitude y satisfies

$$y(t) \equiv 1 \text{ unit}$$

during the entire engagement.

For comparison purposes, the EKF is used to estimate range in the same circumstances. The particular initial condition considered in obtaining the results in Fig. 3.2-3 is

$$\underline{\tilde{x}}_0 = \begin{bmatrix} 225.0 & u \\ 0.703 & u/sec \\ 0.2 & u \\ 0.0 & u/sec \\ 0.0 & ft/sec^2 \end{bmatrix}$$

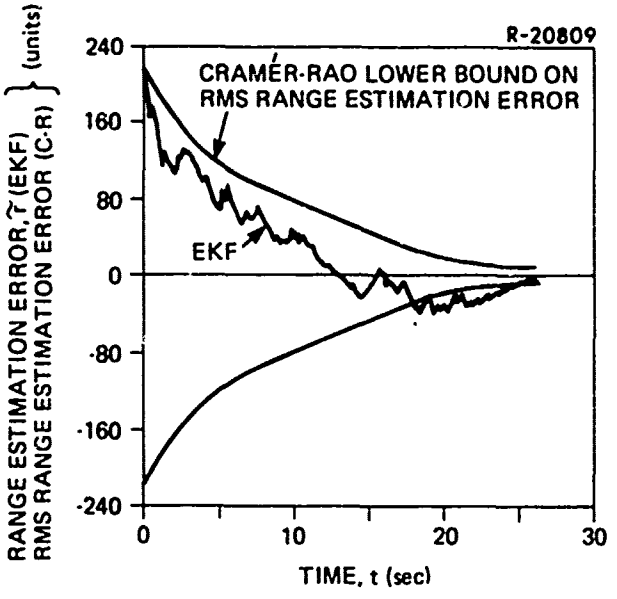

Figure 3.2-3 Application of the Cramér-Rao (C-R) Inequality to the Range Estimation Problem

and the measurement noise sequence, v_k, is the same as in all previous cases. Since the EKF range estimation error, $\tilde{r}$, is well within the Cramér-Rao lower bound on rms range estimation error over most of the trajectory,* it may be inferred that the EKF is quite effective for the range estimation task treated in this study.

3.3 THE QUANTIZED MEASUREMENT CASE

The study of quantization in the LOS angle measurement was performed for the scenario treated in Section 3.2.1, where the initial range estimation error and rms filter range uncertainty are small (-4.67, 4.29 units respectively). The QKF models the quantizer with a random-input describing function that takes into consideration the exact form of the

*The Cramér-Rao lower bound is statistical in nature; i.e., $\tilde{r}$ for any specific trial may be less than the Cramér-Rao lower bound on rms range estimation error, as in Fig. 3.2-3.

nonlinearity and the statistics of the quantizer input, while the EKF accounts for the effect by the artifice of introducing a "fictitious quantization noise" of suitable rms level. The measurement models upon which the EKF and QKF algorithms are based are portrayed in Fig. 2.4-1. The three cases considered in this investigation are specified by quantizer level increments, δ, of 0.5, 1.0 and 2.0 degrees. The number of positive and negative levels, N, is 40, 20 and 10, respectively, so that quantizer saturation occurs at $\pm$20 degrees in each instance.

The small quantization increment, 0.5 deg, leads to the filter performance curves depicted in Fig. 3.3-1. The filter algorithms applied to this problem were the EKF and the QKF-N. During the cruise phase, $t < 7.2$ sec, the performance curves are essentially identical to those obtained without quantization, Fig. 3.2-1. This behavior is to be expected, since the LOS angle is less than 0.25 deg over this period, and the measurement noise is sufficient to mask the effect of the quantizer. Beyond 10 sec, both the QKF and EKF curves are displaced positively with respect to the corresponding range estimation curves obtained without quantization. The peak EKF range estimation error of 11 units at 16 sec is twice that shown in Fig. 3.2-1 at the same time, and the negative peak in $\tilde{r}$ for the QKF-N at 14 sec is reduced from -12 units (without quantization) to -6 units in the present case. The reason for this apparent offset is not clear; extensive monte carlo simulation would be required to determine if biases due to quantization are present. Comparing the results in Figs. 3.2-1 and 3.3-1 (the former corresponding to the same scenario without quantization), there does not seem to be any basis for a judgment concerning the relative statistical performance of the two filter algorithms with or without quantization present.

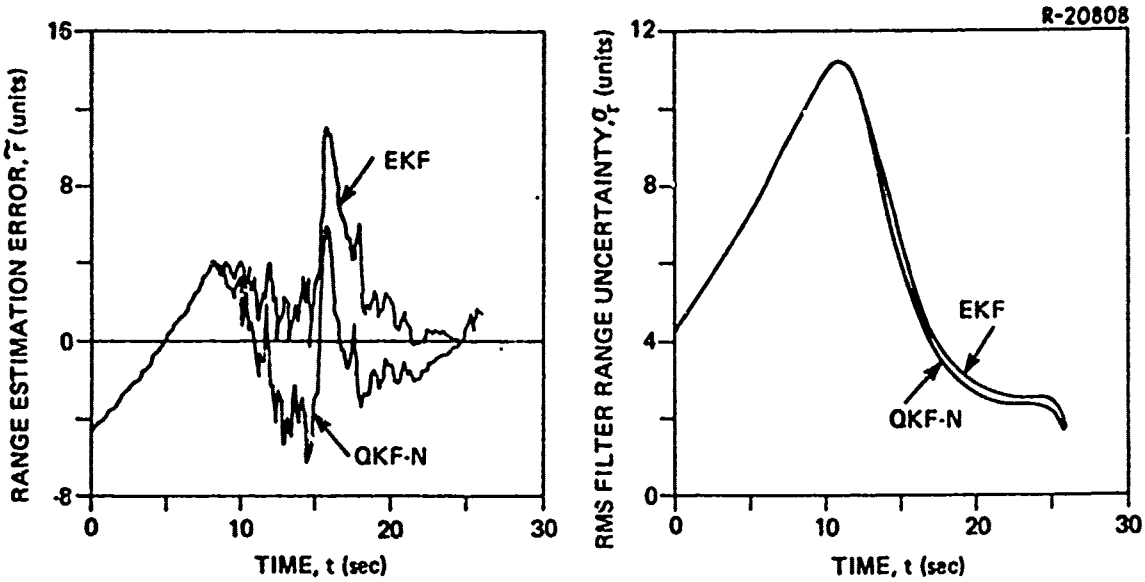

Figure 3.3-1 Range Estimation Algorithm Performance With One-Half Degree LOS Angle Quantization

The filter performance curves for quantizer increments of 1 and 2 deg are given in Fig. 3.3-2. Three filter algorithms were used in these studies, the EKF, QKF-N and QKF-T; observe that the QKF-T was indistinguishable from the QKF-N in its behavior in both cases. Very much the same behavior is observed as in Fig. 3.3-1, in that the first 7.2 sec of the engagement still results in an unchanged time history of $\tilde{r}$, and the QKF curve is generally displaced below the EKF curve of $\tilde{r}$ thereafter.

3.4 SUMMARY

The material presented in this chapter gives an indication of the range estimation capability of two types of filter algorithms, for engagements representing a tactical missile intercepting a surface target after a cruise

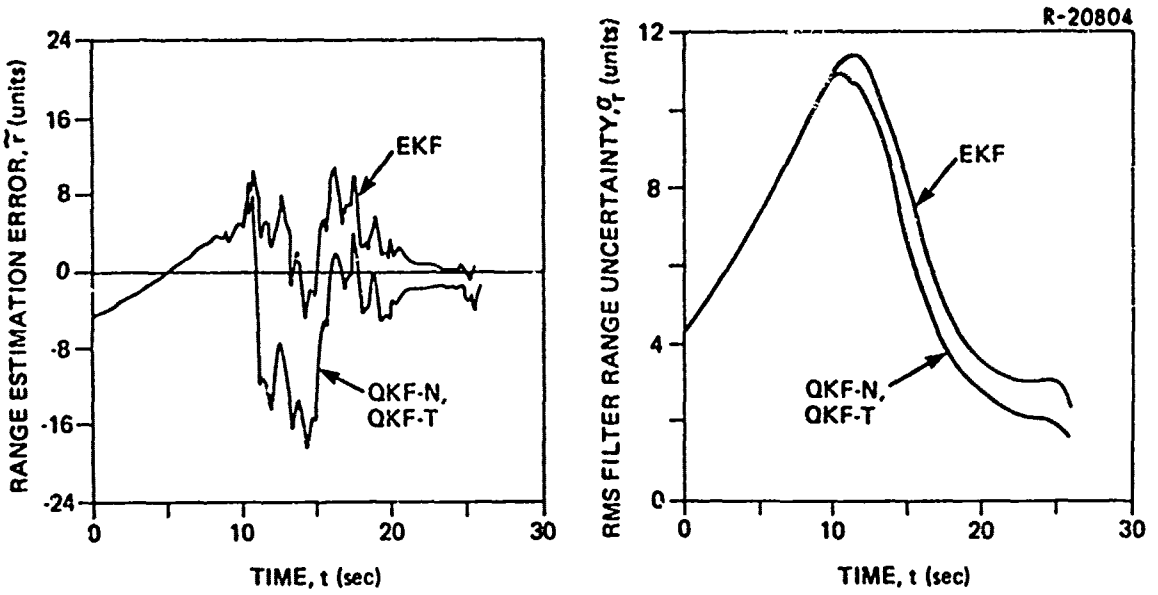

(a) FILTER PERFORMANCE CURVES FOR δ = 1 deg

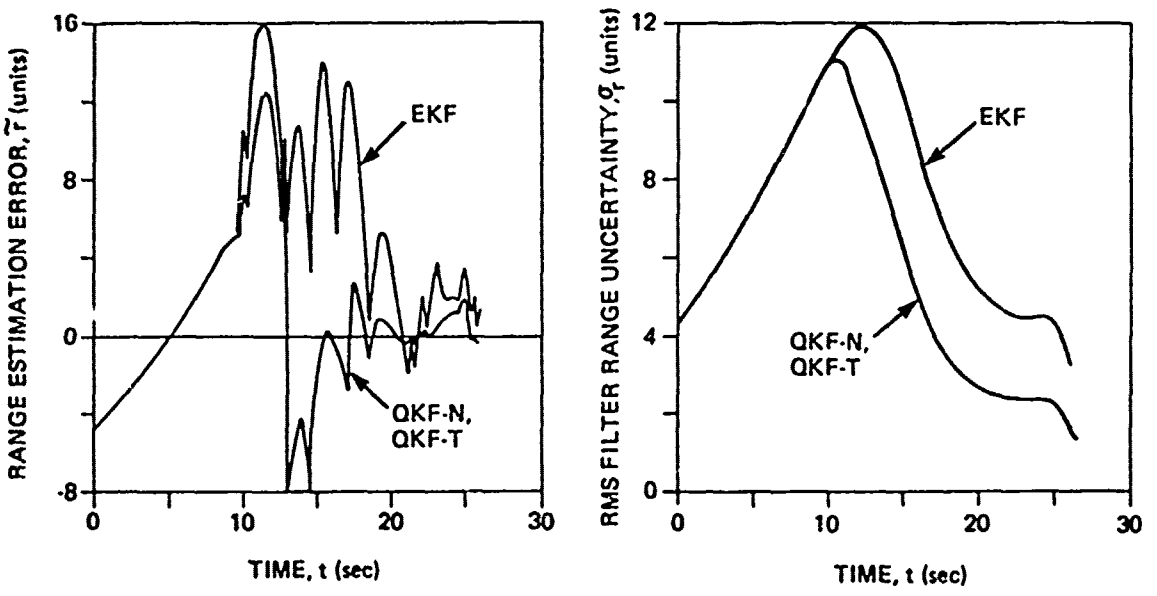

(b) FILTER PERFORMANCE CURVES FOR δ = 2 deg

Figure 3.3-2 Range Estimation Algorithm Performance With One and Two Degree LOS Angle Quantization

(constant altitude) phase. While the design principles of the filter algorithms are quite different, the EKF being derived from small-signal linearization and the QKF being based on quasi-linearization, their performance is quite comparable for small estimation errors (Section 3.2.1). As the mean and rms initial estimation errors are increased, the behavior of the range estimates becomes very dissimilar, especially when the initial estimate is small compared to the true value. However, it is difficult to make a case for the superiority of either algorithm based on the limited number of monte carlo simulations that have been performed.

SUMMARY AND CONCLUSIONS

SUMMARY

Aspects of the passive range estimation problem are considered in this report. Target bearing measurements are taken from a missile that is assumed to follow a trajectory consisting of an initial cruise phase, where the missile flies at constant low altitude, followed by a pitch-up maneuver, during which the missile assumes the desired approach trajectory toward the target. The target is assumed to be constrained to lie on the sea surface. During the cruise phase, target-missile LOS angular excursions are small, providing little range information; the pitch-up maneuver then enhances the missile range estimation capability. The dynamic equations of motion are formulated in Cartesian coordinates, so that they can realistically be assumed to be linear; the nonlinear nature of the task is then restricted to the measurement equation where an inverse tangent relation occurs. An additional source of measurement error that is considered is quantization, illustrated in Fig. 2.4-1a.

Two types of range estimation algorithms are investigated in this effort. The first, the extended Kalman filter (EKF), is based on a linear filter design model obtained by applying small-signal linearization to the measurement nonlinearities. The second is the quasi-linear Kalman filter (QKF), which uses quasi-linear representations of the system nonlinear effects. Three distinct realizations of the QKF, based on different describing function evaluation techniques (Section 2.4), are considered. The primary goal of the study

is to determine how well these different algorithms perform in the scenario described in the above paragraph.

The simulation results are summarized in Chapter 3. In the case with no measurement quantization, filter performance curves for two filter initializations are considered; these are typified by small and large initial rms range estimate uncertainty, σ_r. The presentation for this case is concluded with a discussion of a closely-related subsidiary investigation -- an application of the Cramér-Rao inequality to a simplified intercept scenario. The latter study establishes the lower bound on range estimation error that can be achieved by any algorithm for the problem considered. It thus provides a basis for assessing the performance of the various algorithms in the same case. The chapter concludes with a discussion of the effect of quantization for three quantizer level increments.

4.2 CONCLUSIONS

From the simulation results presented in this report, it appears that the gaussian QKF with numerical integration (i.e., the QKF-N algorithm with describing functions for the arctangent measurement nonlinearity based on the gaussian assumption) performs poorly when initial range estimate errors and rms uncertainties are large (Section 3.2.2). In such cases, the filter makes one large initial correction to the range estimate, and then almost completely ignores subsequent measurement data during the cruise phase, as illustrated in Fig. 3.2-2. This problem is due to the gaussian assumption; the

The figure shows that this adverse behavior is alleviated to a great extent by the QKF-T, which is based on a different probability density function. Despite the fact that the QKF-T does not exhibit the undesirable trait of the QKF-N, the QKF-T algorithm still cannot be said to be superior to the EKF. The QKF-P, based on power series expansion techniques for evaluating describing functions for the arctangent nonlinearity, also did not provide any apparent benefits relative to the EKF.

The Cramér-Rao lower bound on rms estimation error that can be achieved by any algorithm (applied to the cruise phase of the mission in the large initial range uncertainty case, as reported in Section 3.2.3) indicates that the EKF performs nearly as well as possible. If this is true, then the failure of any QKF to outperform the EKF is due to the fact that the EKF is well-suited for the present filtering task; thus it may not be worthwhile to seek more sophisticated filter algorithms (e.g. modified QKF's) for the application considered here.

A second factor contributing to the inability of the QKF methodology to outperform the EKF design technique in this application is that statistical linearization can be very sensitive to the assumptions made regarding the joint probability density function of the system state variables (Refs. 5.6). This problem is especially acute in dealing with nonlinearities such as arctangent(y/x) which exhibit large changes for small changes in input --as happens here for $x \approx 0$. This sensitivity is clearly demonstrated in the performance of the QKF-N and QKF-T (Fig. 3.3-2). It is possible that a more effective QKF algorithm could be found based on other joint probability density functions. However, the Cramér-Rao result outlined above makes it

doubtful that the performance gains obtained in this way would be very significant.

The treatment of quantization (Section 3.3) leads to conclusions that are similar to those discussed above. That is, there does not appear to be performance advantages inherent in any of the filter design techniques considered. Extensive monte carlo analyses of all filter algorithms is needed to make a more definite comparison.

The fact that the QKF approach did not appear to lead to algorithms which perform significantly better than the EKF for the problem considered in this report should not be interpreted to be a general criticism of this application of describing function techniques. It is reasonable to expect that there are applications in which the QKF will excel. In a considerably simpler nonlinear estimation problem (Refs. 2 and 8), definite performance advantages of the QKF were observed. The results presented in this document provide a basis for further research in this area, and give some insight into problem areas that might be encountered and methods of dealing with them.

APPENDIX A

OUTLINE OF NONLINEAR FILTERING THEORY

The equations of the optimal (Kalman) linear filter and of several modified Kalman filters for the nonlinear case for estimating the states of continuous systems using discrete noisy measurement data are reviewed briefly in this appendix. The extended Kalman filter and quasi-linear Kalman filter are suboptimal generalizations of the optimal linear filter, and are applicable to systems which contain significant nonlinear effects such as those encountered in the range estimation problem studied in this report. This appendix provides the background and notational conventions needed for understanding the algorithms applied in this study; a basic familiarity with random variables and state space notation is assumed. Additional detail can be found in Ref. 2.

A.1 KALMAN FILTER EQUATIONS

To apply Kalman filtering to any estimation problem, it is necessary to derive a linear stochastic first-order vector differential equation to model the system, of the form

$$\dot{\underline{x}}(t) = F(t)\underline{x}(t) + G(t)\underline{w}(t) + L(t)\underline{u}(t) \qquad (A.1\text{-}1)$$

where $\underline{x}(t)$ is an $n \times 1$ column vector representing the system state, and $F(t)$ is an $n \times n$ dynamic matrix which defines the

interaction of the state vector components. The vector $\underline{w}(t)$ is a p×1 column vector of white gaussian noise inputs, specified by a zero mean and the spectral density matrix* Q,

$$E[\underline{w}(t)] = 0 \quad ; \quad E[\underline{w}(t)\underline{w}(\tau)^T] = Q(t)\delta(t-\tau)$$

and the matrix G(t) is an n×p distribution matrix which indicates how each component of $\underline{w}(t)$ affects each component of the system state derivative. The variable $\underline{u}(t)$ is an m×1 column vector of known system inputs, which are allocated to the state differential equations by the n×m matrix L(t). In the missile-target range estimation problem considered here, the components of the state vector $\underline{x}$ include position and velocity variables plus target acceleration. Note that F, G, L and Q matrices may be time-varying; in subsequent development the explicit notation (t) will be omitted.

At discrete instants of time, t_k, measurements of linear combinations of the state variables are made. The equation describing this measurement process has the general form

$$\underline{z}_k = H_k\underline{x}_k + \underline{v}_k \qquad (A.1\text{-}2)$$

where $\underline{z}_k$ is a vector of r measured quantities at time t_k, H_k is an r×n observation matrix describing the linear combinations of state variables which comprise $\underline{z}_k$ in the absence of noise, and $\underline{v}_k$ is an r-vector of zero-mean gaussian measurement errors with a covariance matrix, R_k, defined by†

*The symbol $\delta(t-\tau)$ denotes the Dirac delta function.

†The symbol δ_{jk} is the Kronecker delta; it is unity for j=k and zero otherwise.

$$E\left[\underline{v}_k \underline{v}_j^T\right] = R_k \delta_{jk}$$

The objective of optimal estimation theory is to process the measurements in real time and produce an estimate $\underline{\hat{x}}(t)$ of the system state $\underline{x}(t)$ having minimum error, in some statistical sense. The optimization criterion most often chosen is that of minimizing the mean square estimation error. This estimate is calculated with the Kalman filtering algorithm.

As each new measurement becomes available, there is essentially an instantaneous change in the knowledge of the state $\underline{x}(t_k)$. Denoting the optimum estimate of $\underline{x}(t_k)$ just prior to the availability of $\underline{z}_k$ as $\underline{\hat{x}}_k(-)$ and the optimum estimate of the state vector immediately after processing $\underline{z}_k$ as $\underline{\hat{x}}_k(+)$, the Kalman filter generates the optimum estimate of the system state according to the following algorithm:

$$\dot{\underline{\hat{x}}}(t) = F\underline{\hat{x}}(t) + L\underline{u}(t) \; ; \; \underline{\hat{x}}(t_{k-1}) = \underline{\hat{x}}_{k-1}(+) \; , \; t_{k-1} \leq t \leq t_k \tag{A.1-3}$$

$$\underline{\hat{x}}_k(+) = \underline{\hat{x}}_k(-) + K_k\left[\underline{z}_k - H_k\underline{\hat{x}}_k(-)\right] \tag{A.1-4}$$

Equation (A.1-3) is used to propagate the estimate between measurements, and Eq. (A.1-4) is used to update the estimate when new data is received.

The n×r matrix K_k in Eq. (A.1-4) is the Kalman gain matrix, which is obtained from the estimation error covariance matrix, P, as follows:

$$K_k = P_k(-)H_k^T\left[H_kP_k(-)H_k^T + R_k\right]^{-1} \tag{A.1-5}$$

The matrix P satisfies the propagation and update equations given in Ref. 2 as

$$\dot{P}(t) = FP + PF^T + GQG^T \quad , \quad t_{k-1} \leq t \leq t_k$$
$$P_k(+) = [I - K_k H_k]P_k(-) \qquad \text{(A.1-6)}$$

These relations complete the outline of the Kalman filter design for linear systems.

A.2 THE EXTENDED KALMAN FILTER FOR NONLINEAR ESTIMATION

Optimal linear estimation theory provides a powerful analytical tool for analyzing and synthesizing filter algorithms when the system equations of motion and measurement equations are linear. However, the range estimation problem contains at least one inherent nonlinear effect which may be sufficiently important to warrant the use of a nonlinear estimation technique. This effect is the LOS angle or bearing measurement provided by the target tracking system sensor, which is a nonlinear function of relative missile-target position in Cartesian coordinates. Whenever nonlinearities are not negligible, a data processing algorithm derived from the principles of nonlinear estimation theory may yield considerably better estimates than a linear (or linearized) Kalman filter. This section discusses the extended Kalman filter used in this report as one solution to the nonlinear range estimation problem.

A quite general mathematical model for nonlinear stochastic systems is given by the equations

$$\dot{\underline{x}}(t) = \underline{f}(\underline{x}(t),t) + G(t)\underline{w}(t) + L(t)\underline{u}(t) \qquad \text{(A.2-1)}$$

$$\underline{z}_k = \underline{h}_k(\underline{x}(t_k)) + \underline{v}_k \quad ; \quad k = 1,2,... \qquad \text{(A.2-2)}$$

where $\underline{f}$ and $\underline{h}_k$ are nonlinear differentiable* functions of the state vector $\underline{x}$, $\underline{w}(t)$ and $\underline{v}_k$ are zero mean, independent gaussian white noise processes having spectral density and covariance matrices $Q(t)$ and R_k, respectively, and $\underline{u}$ is a vector of known inputs. Assume as before that measurements are taken at discrete times t_k.

The first approach one might use to derive a filtering algorithm for $\underline{x}(t)$ in Eq. (A.2-1) is to linearize the nonlinear functions $\underline{f}$ and $\underline{h}_k$ about an appropriate known reference trajectory $\bar{\underline{x}}(t)$ and then apply conventional optimal linear estimation theory -- i.e., the Kalman filter discussed in the last section. Thus, denoting $\bar{\underline{x}}(t_k)$ by $\bar{\underline{x}}_k$, the so-called small-signal linearization procedure results in the expressions

$$\underline{f}(\underline{x},t) \cong \underline{f}(\bar{\underline{x}},t) + \left.\frac{\partial \underline{f}}{\partial \underline{x}}\right|_{\underline{x}=\bar{\underline{x}}} (\underline{x}-\bar{\underline{x}})$$

$$\triangleq \underline{f}(\bar{\underline{x}},t) + F(\bar{\underline{x}},t)(\underline{x}-\bar{\underline{x}}) \qquad \text{(A.2-3)}$$

$$\underline{h}_k(\underline{x}_k) \cong \underline{h}_k(\bar{\underline{x}}_k) + \left.\frac{\partial \underline{h}_k}{\partial \underline{x}_k}\right|_{\underline{x}_k=\bar{\underline{x}}_k} (\underline{x}_k-\bar{\underline{x}}_k)$$

$$\triangleq \underline{h}_k(\bar{\underline{x}}_k) + H_k(\bar{\underline{x}}_k)(\underline{x}_k-\bar{\underline{x}}_k) \qquad \text{(A.2-4)}$$

*Note that differentiability, as required in Eqs. (A.2-3) and (A.2-4), precludes the formal application of the present technique to systems with nonlinearities such as the limiter and the quantizer which do not have derivatives everywhere.

which may be substituted into Eqs. (A.2-1) and (A.2-2) to derive the corresponding Kalman filter which estimates the variation in $\underline{x}$, $\Delta\underline{x}(t) \triangleq \underline{x}(t) - \bar{\underline{x}}(t)$, from the reference trajectory. When the reference trajectory is chosen to be the current best estimate of the state $\underline{x}(t)$, the resulting algorithm is known as an extended Kalman filter (EKF); the mechanization equations for the latter are given in Table A.2-1 (Ref. 2).

TABLE A.2-1

SUMMARY OF THE DISCRETE/CONTINUOUS EXTENDED KALMAN FILTER ALGORITHM

System Model	$\dot{\underline{x}} = \underline{f}(\underline{x},t) + G(t)\underline{w}(t) + L(t)\underline{u}(t)$; $E\left[\underline{w}(t)\underline{w}^T(\tau)\right] = Q(t)\delta(t-\tau)$
Measurement Model	$\underline{z}_k = \underline{h}_k(\underline{x}_k) + \underline{v}_k$, $k=1,2,\ldots$; $E\left[\underline{v}_k\underline{v}_j^T\right] = R_k\delta_{jk}$
Initial Conditions	$E[\underline{x}(0)] = \hat{\underline{x}}_0$, $E\left[(\underline{x}(0)-\hat{\underline{x}}_0)(\underline{x}(0)-\hat{\underline{x}}_0)^T\right] = P_0$
Other Assumptions	$E\left[\underline{w}(t)\underline{v}_k^T\right] = 0$ for all k and all t $\underline{u}(t)$ is a known input vector
State Estimate Extrapolation	$\dot{\hat{\underline{x}}} = \underline{f}(\hat{\underline{x}},t) + L(t)\underline{u}(t)$; $\hat{\underline{x}}(t_{k-1}) = \hat{\underline{x}}_{k-1}(+)$
Error Covariance Extrapolation	$\dot{P} = F(\hat{\underline{x}},t)P + PF^T(\hat{\underline{x}},t) + G(t)Q(t)G^T(t)$; $P(t_{k-1}) = P_{k-1}(+)$
State Estimate Update	$\hat{\underline{x}}_k(+) = \hat{\underline{x}}_k(-) + K_k\left[\underline{z}_k - \underline{h}_k(\hat{\underline{x}}_k(-))\right]$
Error Covariance Update	$P_k(+) = \left[I-K_kH_k(\hat{\underline{x}}_k(-))\right]P_k(-)$
Gain Matrix	$K_k = P_k(-)H_k^T\left[H_kP_k(-)H_k^T + R_k\right]^{-1}$
Definitions	$F(\hat{\underline{x}},t) \triangleq \left.\frac{\partial\underline{f}(\underline{x},t)}{\partial\underline{x}}\right\vert_{\underline{x}=\hat{\underline{x}}}$ $H_k \triangleq \left.\frac{\partial\underline{h}_k(\underline{x}_k)}{\partial\underline{x}_k}\right\vert_{\underline{x}_k=\hat{\underline{x}}_k(-)}$

As long as the linearization in Eq. (A.2-4) is accurate, the filter algorithm will give nearly optimal performance. Experience with similar ranging problems indicates that the EKF is an adequate suboptimal estimation technique in applications in which estimation error is small.

A.3 THE QUASI-LINEAR KALMAN FILTER FOR NONLINEAR ESTIMATION

As in the previous section, the general mathematical model is assumed to be of the form indicated in Eqs. (A.2-1) and (A.2-2), with the removal of the restriction that $\underline{f}$ and $\underline{h}$ must be differentiable. The point of departure is the method of linearization: Rather than assuming that estimation error is "small" in some sense and making use of the small-signal linearization technique, it is assumed that the estimation error vector $\tilde{\underline{x}}$ is a zero-mean gaussian random variable with covariance P, and the nonlinearities in the model are replaced with their approximate random-input describing function (ridf) representations. The quasi-linear analogs to the approximations in Eqs. (A.2-3) and (A.2-4) are

$$\underline{f}(\underline{x},t) \cong \underline{f}(\hat{\underline{x}},P,t) + N_f(\hat{\underline{x}},P,t)(\underline{x}-\hat{\underline{x}})$$

$$\underline{h}_k(\underline{x}_k(-)) \cong \hat{\underline{h}}_k(\hat{\underline{x}}_k(-),P_k(-)) + N_{h,k}(\hat{\underline{x}}_k(-),P_k(-))(\underline{x}_k-\hat{\underline{x}}_k(-)) \qquad \text{(A.3-1)}$$

where

$$\hat{\underline{f}}(\hat{\underline{x}},P,t) \triangleq \left[(2\pi)^n|P|\right]^{-\frac{1}{2}} \int_{-\infty}^{\infty}\cdots\int \underline{f}(\underline{x},t)\exp\left\{-\tfrac{1}{2}\tilde{\underline{x}}^T P^{-1}\tilde{\underline{x}}\right\} dx_1 dx_2 \ldots dx_n$$

$$N_f(\hat{\underline{x}},P,t) \triangleq \left[(2\pi)^n|P|\right]^{-\frac{1}{2}} \int_{-\infty}^{\infty}\cdots\int \underline{f}(\underline{x},t)\exp\left\{-\tfrac{1}{2}\tilde{\underline{x}}^T P^{-1}\tilde{\underline{x}}\right\} P^{-1}\tilde{\underline{x}}\, dx_1 dx_2 \ldots dx_n \qquad \text{(A.3-2)}$$

and the arrays $\hat{\underline{h}}_k$, $N_{h,k}$ are defined in a similar way with $\underline{h}_k$ substituted for $\underline{f}$ in Eq. (A.3-2).

For further details on the above statistical linearization procedure, see Refs. 3 and 5. In the present context, it suffices to observe that the gaussian assumption guarantees that the ridf arrays in Eq. (A.3-1) are functions only of $\hat{\underline{x}}$, P and t, as the notation suggests. For small estimation error (for P small), the quasi-linear approximation approaches small-signal linearization; when the deviation of $\hat{\underline{x}}$ from $\underline{x}$ is not insignificant, then P provides the statistical measure ("amplitude") of this deviation, and the ridf representations of $\underline{f}$ and $\underline{h}$ are dependent on this amplitude in a way which captures the nonlinear effect much more faithfully than the small-signal linearized model.

The use of the quasi-linear approximations indicated in Eqs. (A.3-1) and (A.3-2) as the basis for a modified Kalman filter algorithm leads to the quasi-linear Kalman filter (QKF). The equations are directly analogous to those given in Table A.2-1 with the following substitutions:

$$\begin{aligned}
\underline{f}(\hat{\underline{x}},t) &\rightarrow \hat{\underline{f}}(\hat{\underline{x}},P,t) \\
F(\hat{\underline{x}},t) &\rightarrow N_f(\hat{\underline{x}},P,t) \\
\underline{h}_k(\hat{\underline{x}}_k(-)) &\rightarrow \hat{\underline{h}}(\hat{\underline{x}}_k(-),P_k(-)) \\
H_k &\rightarrow N_{h,k}(\hat{\underline{x}}_k(-),P_k(-))
\end{aligned} \qquad \text{(A.3-3)}$$

The algorithm obtained by making the changes indicated in Eq. (A.3-3) in Table A.2-1 completes the development of the QKF.

APPENDIX B

RANDOM-INPUT DESCRIBING FUNCTIONS FOR THE RANGE ESTIMATION MEASUREMENT NONLINEARITIES

B.1 INTRODUCTION

Two nonlinearities are treated in this investigation: $\tan^{-1}(y/x)$, which is encountered in expressing LOS angle (target bearing) in terms of missile-target separation in Cartesian coordinates, and $f_q(z)$, or the quantizer defined in Eq. (2.3-6). The quasi-linear representation of the quantizer (Eqs. (2.4-13) to (2.4-15)) is a well-known result, so it is not presented here (cf. Ref. 3). The arctangent nonlinearity has not been treated extensively prior to this study (refer to Ref. 6 for a preliminary approximate approach), so it is considered in some detail.

The random-input describing function (ridf) approximation sought is of the form

$$\begin{aligned}\theta(x,y) &\triangleq \tan^{-1}(y/x)\\ &\cong \hat{\theta} + n_x(x-\hat{x}) + n_y(y-\hat{y})\\ &\triangleq \hat{\theta} + \underline{n}^T(\underline{x}-\underline{\hat{x}})\end{aligned} \qquad \text{(B.1-1)}$$

where

$$\begin{aligned}\underline{x}^T &\triangleq [x\ y]\\ \underline{\hat{x}}^T &\triangleq [\hat{x}\ \hat{y}]\\ \hat{\theta} &\triangleq E[\theta(\underline{x})]\\ \underline{n}^T &\triangleq E[\theta(\underline{x})(\underline{x}-\underline{\hat{x}})^T]P^{-1}\end{aligned} \qquad \text{(B.1-2)}$$

and it is assumed that the vector $\underline{x}$ is gaussian with mean, $\hat{\underline{x}}$, and covariance, P, given by

$$P = E\left[(\underline{x}-\hat{\underline{x}})(\underline{x}-\hat{\underline{x}})^T\right]$$

$$= \begin{bmatrix} p_{xx} & p_{xy} \\ p_{xy} & p_{yy} \end{bmatrix} \qquad \text{(B.1-3)}$$

The evaluation of $\underline{n}$ is simplified under the gaussian assumption (Ref. 5) to be

$$\underline{n}^T = \frac{\partial\hat{\theta}}{\partial\hat{\underline{x}}} \qquad \text{(B.1-4)}$$

However, the integral required in evaluating $\hat{\theta}$, as specified in Eq. (B.1-2), i.e.,

$$\hat{\theta} = \frac{1}{2\pi|P|^{\frac{1}{2}}} \int_{-\infty}^{\infty}\int_{-\infty}^{\infty} \tan^{-1}(y/x)\, \exp\left\{-\tfrac{1}{2}(\underline{x}-\hat{\underline{x}})^T P^{-1}(\underline{x}-\hat{\underline{x}})\right\} dxdy \qquad \text{(B.1-5)}$$

cannot be performed analytically to yield a closed-form solution, so other approaches to evaluating Eq. (B.1-2) are required.

B.2 AN APPROXIMATE QUASI-LINEAR REPRESENTATION OF ARCTAN(y/x)

A technique that gives rise to approximate ridf's for use in Eq. (B.1-1) is based on the series expansion of the nonlinearity. In general, given

$$f(\underline{x}) = f(\hat{\underline{x}}) + \frac{\partial f}{\partial x}\bigg|_{\underline{x}=\hat{\underline{x}}} (x-\hat{x}) + \frac{\partial f}{\partial y}\bigg|_{\underline{x}=\hat{\underline{x}}} (y-\hat{y})$$

$$+ \tfrac{1}{2}\left\{\frac{\partial^2 f}{\partial x^2}\bigg|_{\underline{x}=\hat{\underline{x}}} (x-\hat{x})^2 + 2\,\frac{\partial^2 f}{\partial x \partial y}\bigg|_{\underline{x}=\hat{\underline{x}}} (x-\hat{x})(y-\hat{y})\right.$$

$$\left. + \frac{\partial^2 f}{\partial y^2}\bigg|_{\underline{x}=\hat{\underline{x}}} (y-\hat{y})^2\right\}$$

$$+ \text{higher order terms} \qquad \text{(B.2-1)}$$

the expectation operation yields

$$E[f(\underline{x})] = f(\hat{\underline{x}}) + \tfrac{1}{2}\left\{\frac{\partial^2 f}{\partial x^2}\bigg|_{\underline{x}=\hat{\underline{x}}} p_{xx} + 2\,\frac{\partial^2 f}{\partial x \partial y}\bigg|_{\underline{x}=\hat{\underline{x}}} p_{xy}\right.$$

$$\left. + \frac{\partial^2 f}{\partial y^2}\bigg|_{\underline{x}=\hat{\underline{x}}} p_{yy}\right\}$$

$$+ \text{higher order terms} \qquad \text{(B.2-2)}$$

If the elements of P are not large with respect to $\hat{x}$ and $\hat{y}$ (i.e., if the estimation error uncertainty is small in comparison with the estimates of missile-target separation), then a useful approximation is obtained by omitting the higher order terms in Eq. (B.2-2). For arctan(y/x) this leads to

$$\hat{\theta} \cong \hat{\theta}_p \triangleq \tan^{-1}(\hat{y}/\hat{x}) + [\hat{x}\hat{y}(p_{xx}-p_{yy}) - p_{xy}(\hat{x}^2 - \hat{y}^2)]/(\hat{x}^2+\hat{y}^2)^2 \qquad \text{(B.2-3)}$$

Observe that substituting the first term of Eq. (B.2-3) into Eqs. (B.1-2) and (B.1-4) yields the small-signal linearization approximation given in Eq. (2.4-1),

$$\theta(\underline{x}) \cong \theta(\hat{\underline{x}}) + \left.\frac{\partial\theta}{\partial x}\right|_{\underline{x}=\hat{\underline{x}}} (x-\hat{x}) + \left.\frac{\partial\theta}{\partial y}\right|_{\underline{x}=\hat{\underline{x}}} (y-\hat{y}) \qquad \text{(B.2-4)}$$

The second term in Eq. (B.2-3) represents the first correction term which accounts for the estimation error uncertainty. This approximate expression for $\hat{\theta}$, and the approximate values of n_x and n_y obtained by applying Eq. (B.1-4), should quite accurately represent the amplitude-dependent nature of the arctangent nonlinearity in cases where rms estimation uncertainty is moderate with respect to $\hat{\underline{x}}$.

B.3 EVALUATION OF RIDF'S BY NUMERICAL INTEGRATION

Although the integrals involved in determining the expected values indicated in Eq. (B.1-2) cannot be evaluated analytically in closed form, useful results can be obtained by direct numerical integration. The implementation of numerical solutions to Eq. (B.1-2) proceeds as follows: Given the input means $(\hat{x},\hat{y})$ and covariances (p_{xx}, p_{yy}, p_{xy}) of the gaussian random variables (x,y), first determine the lower triangular transform matrix T,

$$\underline{u} = \begin{bmatrix} u \\ v \end{bmatrix} \triangleq T(\underline{x}-\hat{\underline{x}}) \qquad \text{(B.3-1)}$$

which results in $\underline{u}$ being a zero-mean gaussian random variable with covariance

$$E\left[\underline{u}\underline{u}^T\right] = \begin{bmatrix} 1 & 0 \\ 0 & 1 \end{bmatrix} \triangleq P_u \qquad \text{(B.3-2)}$$

This operation thus transforms ellipses of constant probability,

$$(\underline{x}-\hat{\underline{x}})^T P^{-1} (\underline{x}-\hat{\underline{x}}) = \text{constant}$$

in the (x,y) plane into circles centered on the origin of the (u,v) plane. The (u,v) plane is then divided into $n_r \times n_\phi$ cells in polar coordinates, as shown in Fig. B.3-1. The center of each cell is then accorded a weighting which depends only on the gaussian assumption and on its radial distance from the origin; the cells bounded by $(j-1)\Delta r$ and $j\Delta r$ have the weighting

$$w_j = \frac{1}{\sqrt{2\pi}} \exp(-\tfrac{1}{2}(j-\tfrac{1}{2})^2 \Delta r^2) \qquad \text{(B.3-3)}$$

Integration is completed in the (u,v) plane by summing over the cells,

$$\hat{\theta} \cong \hat{\theta}_N \triangleq \sum_{j=1}^{n_r} w_j \sum_{k=1}^{n_\phi} \tan^{-1}\left(\frac{y(u_{jk}, v_{jk})}{x(u_{jk}, v_{jk})}\right) \qquad \text{(B.3-4)}$$

where

$$u_{jk} = (j-\tfrac{1}{2})\Delta r \cos(\phi_k)$$

$$v_{jk} = (j-\tfrac{1}{2})\Delta r \sin(\phi_k)$$

$$\phi_k = 2\pi(k-1)/n_\phi \qquad \text{(B.3-5)}$$

and x and y are found by inverting Eq. (B.3-1),

R-19431

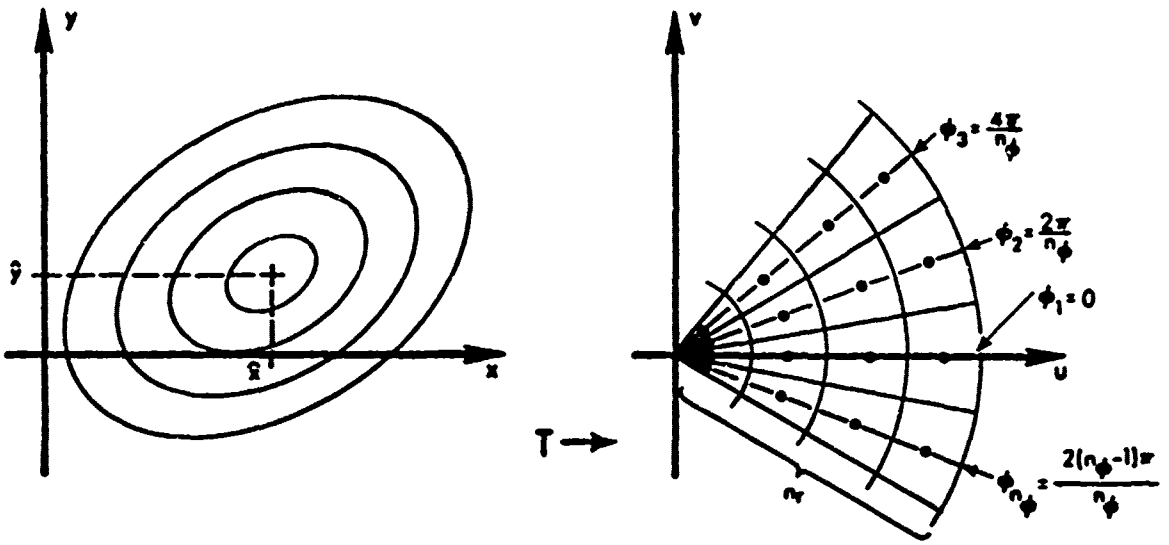

Figure B.3-1 Transformation of Variables for Numerical Integration of Random-Input Describing Functions

$$x(u_{jk},v_{jk}) = \left[\sqrt{p_{xx}p_{yy}-p_{xy}^2}\ u_{jk} + p_{xy}v_{jk}\right] \Big/ \sqrt{p_{yy}} + \hat{x}$$

$$y(u_{jk},v_{jk}) = \sqrt{p_{yy}}\ v_{jk} + \hat{y} \qquad \text{(B.3-6)}$$

The numerical integration of $E[(\underline{x}-\hat{\underline{x}})\theta]$ required for the evaluation of the random component ridf's as indicated in Eq. (B.1-2) is performed in a directly analogous manner.

Observe that this technique is perfectly general with respect to the assumed joint probability density function (pdf) of x and y. If the gaussian joint pdf is denoted p(x,y),

then the truncated gaussian pdf upon which the QKF-T is based is defined by

$$p_T(x,y) = \begin{cases} p(x,y) + p(-x,y) & , \quad x \geq 0 \\ 0 & , \quad x < 0 \end{cases} \qquad \text{(B.3-7)}$$

The same numerical integration subroutine which evaluates $\hat{\theta}_N$, Eq. (B.3-4), was thus simply modified to calculate $\hat{\theta}_T$, or $\hat{\theta}$ based on the joint pdf given in Eq. (B.3-7), for use in the QKF-T algorithm.

Figure B.3-2 portrays the evaluation of $\hat{\theta}$ by numerical integration, $\hat{\theta}_N$, for 90 cells (n_r=5, n_ϕ=18) and for 360 cells (n_r=10,n_ϕ=36), for various values of estimated horizontal separation, $\hat{x}$. Based on the small deviations between these results, it is judged that 90-cell numerical integration is adequate for this application. The plots $\hat{\theta}_T$, $\hat{\theta}_p$ (corresponding to the result obtained by applying Eq. (B.2-3)), and $\theta(\underline{\hat{x}})$, corresponding to the use of small-signal linearization, Eq. (2.4-1), are also depicted for the sake of comparison. Note that as $\hat{x}$ becomes large (relative to the estimation uncertainty), the three approaches are very nearly equivalent. The largest deviation between $\theta(\hat{x})$ and $\hat{\theta}_N$ with this value of p_{xx} occurs for $\hat{x} \cong \sqrt{p_{xx}}$; at that distance, $\hat{\theta}_N$ is 11 times larger than $\theta(\hat{x})$. The power series approach for obtaining approximate ridf's presented in Section B.2 leads to $\hat{\theta}_p$, which essentially diverges for small $\hat{x}$. This effect for small estimated horizontal separation may not be critical, since the missile will no longer be in a cruise phase when it is so close to the target. In the middle range of $\hat{x}$, however, the disparity between $\hat{\theta}_p$ and $\hat{\theta}_N$ is also quite large -- $\hat{\theta}_N$ is as much as 6 times larger than $\hat{\theta}_p$ -- which indicates that $\hat{\theta}_p$ may not be a useful approximate ridf. On the other hand, since $\hat{\theta}_p$ is between $\theta(\underline{\hat{x}})$ and $\hat{\theta}_N$ for all $\hat{x}$ greater than 8 units, a quasi-linear Kalman filter based on series-approximate ridf's can be

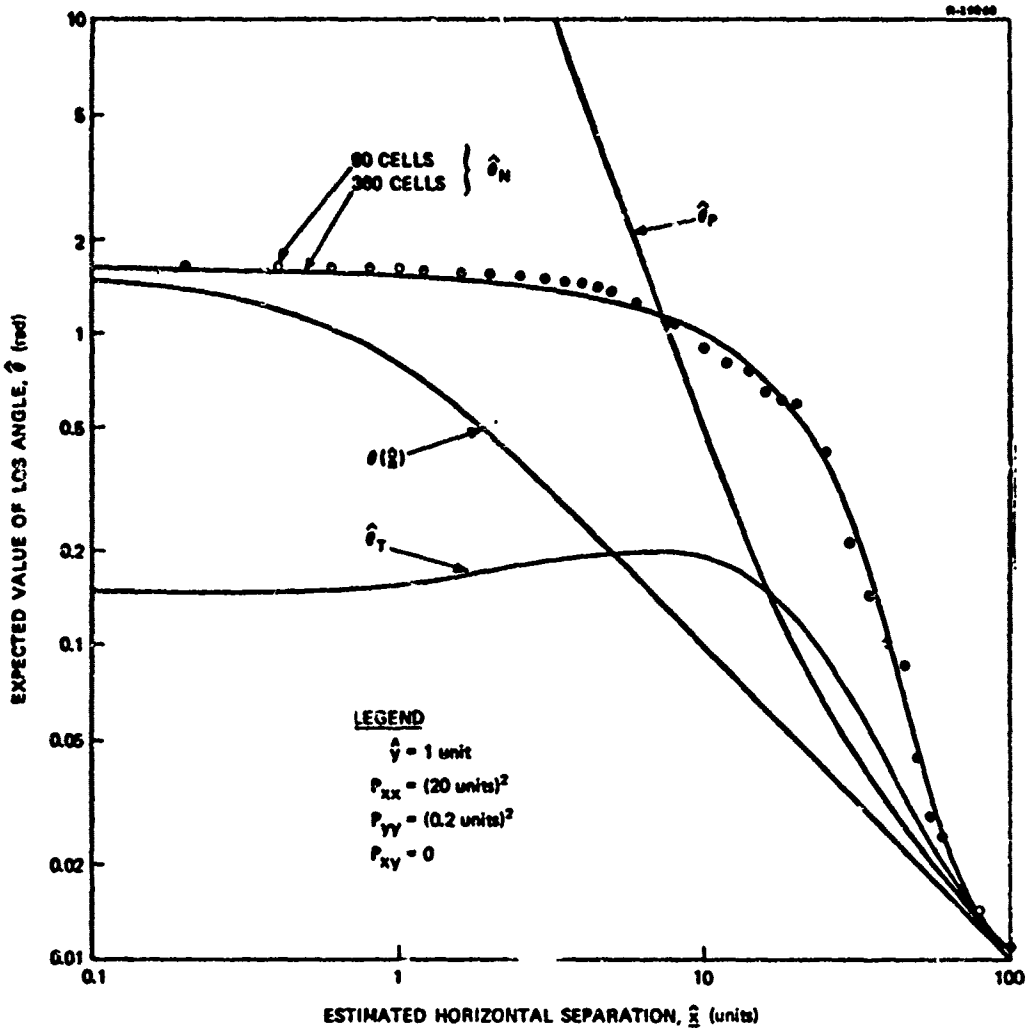

Figure B.3-2 Arctangent(y/x) ridf s by Numerical Integration and Power Series Approximation

expected to exhibit a performance that is intermediate to the EKF (based on $\theta(\underline{\hat{x}})$) and the accurate QKF (based on $\hat{\theta}_N$), so the fact that $\hat{\theta}_P$ is not an accurate ridf may not be detrimental in this application. The nongaussian-based ridf, $\hat{\theta}_T$, behaves most like $\hat{\theta}_P$ for moderate and large $\hat{x}$ ($\hat{x} \geq \sqrt{P_{xx}}$); as x decreases, $\hat{\theta}_T$ remains small compared with the other results.

It may be of interest to compare the computer time expenditure required by the EKF, QKF-P and QKF-N: A simulation of a single engagement of the type considered in Chapter 3 necessitates 135 evaluations of $\theta(\hat{\underline{x}})$, $\hat{\theta}_P$ or $\hat{\theta}_N$, respectively; the corresponding data processing times are 1.74 min, 1.81 min (+3.7 percent), and 2.17 min (+24.5 percent), where the percentage increases indicated for the QKF-P and QKF-N are defined with respect to the EKF. Thus the computational burden for the QKF-N is not a significant problem.

Sections B.2 and B.3 have summarized two approaches used to generate quasi-linear representations for the measurement arctangent nonlinearity. The results presented in Chapter 3 demonstrate the performance that can be achieved using the ridf's derived in this appendix as the basis for the design of a quasi-linear Kalman filter to estimate missile-target range from measurements of LOS angle.

REFERENCES

1. Brown, C.M., Jr., Price, C.F. and Licata, W.H., "Inertially Aided Ranging for Guidance Systems," AIAA Guidance and Control Conference, Boston, Mass., August 1975.

2. Gelb, A. (Ed.), Applied Optimal Estimation, The MIT Press, Cambridge, Mass., 1974.

3. Gelb, A. and Vander Velde, W.E., Multiple-Input Describing Functions and Nonlinear System Design, McGraw-Hill Book Co., New York, 1968.

4. Widrow, B., "Statistical Analysis of Amplitude-Quantized Sampled-Data Systems," Trans. American Institute of Electrical Engineers, Pt. II, pp. 555-568, 1960.

5. Taylor, J.H., "Handbook for the Direct Statistical Analysis of Missile Guidance Systems Via CADET™," The Analytic Sciences Corp., Report No. TR-385-2, 31 May 1975.

6. Taylor, J.H. and Price, C.F., "Direct Statistical Analysis of Missile Guidance Systems Via CADET™," The Analytic Sciences Corp., Report No. TR-385-3, to be published.

7. Van Trees, H.L., Detection, Estimation, and Modulation Theory, Part I, John Wiley and Sons, Inc., New York, 1968.

8. Phaneuf, R.J., "Approximate Nonlinear Estimation," Ph.D. Thesis, Dept. of Aeronautics and Astronautics, M.I.T., Cambridge, Mass., May 1968.